

OXYGEN ABSORPTION IN M87: EVIDENCE FOR A WARM+HOT ISM

DAVID A. BUOTE¹

UCO/Lick Observatory, University of California at Santa Cruz, Santa Cruz, CA 95064; buote@ucolick.org

Accepted for Publication in The Astrophysical Journal

ABSTRACT

We present a re-analysis of the *ROSAT* PSPC data within the central 100 kpc of M87 to search for intrinsic oxygen absorption similar to that recently measured in several galaxies and groups. Since M87 is the brightest nearby galaxy or cluster possessing an average temperature (~ 2 keV) within the PSPC bandpass, it is the ideal target for this study. Using a spatial-spectral deprojection analysis we find the strongest evidence to date for intrinsic oxygen absorption in the hot gas of a galaxy, group, or cluster. Single-phase plasma models modified by intervening Galactic absorption cannot fit the 0.2-2.2 keV PSPC data as they under-predict the 0.2-0.4 keV region and over-predict the 0.5-0.8 keV region where the emission and absorption residuals are obvious upon visual inspection of the spectral fits. These absorption and emission features are significant out to the largest radii investigated. Since the excess emission between 0.2-0.4 keV rules out intrinsic absorption from cold gas or dust, the most reasonable model for the excess emission and absorption features is warm, collisionally ionized gas with a temperature of $\sim 10^6$ K. Simple multiphase models (cooling flow, two phases) modified by both intervening Galactic absorption and by a single oxygen edge provide good fits and yield temperatures and Fe abundances of the hot gas that agree with previous determinations by *ASCA* and *SAX*.

The multiphase models of M87 inferred from the PSPC can account for the excess EUV emission observed with *EUVE* and the excess X-ray absorption inferred from *Einstein* and *ASCA* data above 0.5 keV. This evidence for a multiphase warm+hot ISM in M87 essentially confirms the original detection by Canizares et al. within the central $\sim 2'$ using the *Einstein* FPCS. Although the total mass of the warm gas implied by the oxygen absorption is consistent with the matter deposited by a cooling flow, the suppression of the mass deposition rate and the distortion of the X-ray isophotes in the region where the radio emission is most pronounced suggest some feedback effect from the AGN on the cooling gas.

Subject headings: cooling flows – intergalactic medium – X-rays: galaxies

1. INTRODUCTION

A contentious issue in X-ray astronomy, and more generally in the study of galaxy formation and evolution, is whether massive galaxies, groups, and clusters possess inhomogeneous cooling flows wherein large quantities of gas have cooled and dropped out of the hot phase resulting in a spatially extended multiphase medium (e.g., Fabian, Nulsen, & Canizares 1984; Fabian 1994; Binney 1996). In the era before *Chandra* and *XMM* the instrument with the best combined spatial resolution, bandwidth, and energy resolution for studies of cooling flows was the *ROSAT* PSPC. The bandwidth (0.1-2.4 keV) of the PSPC is especially critical because its sensitivity to energies both above and below the O I edge (0.532 keV) has allowed us recently to detect intrinsic oxygen absorption in cooling flow galaxies and groups which provides the first direct evidence of a spatially extended multiphase medium in these systems (Buote 2000b, hereafter PAPER1; Buote 2000d, hereafter PAPER3).

M87 is arguably the best target for study of its hot plasma with *ROSAT* because it is the brightest nearby galaxy, group, or cluster that also possesses an ambient gas temperature (~ 2 keV) that lies within the bandpass of the PSPC. For these reasons M87 has been the subject of numerous X-ray studies. The early analysis by Canizares et al (1982) of the *Einstein* FPCS spectral data of M87

provided the first evidence of a multiphase hot ISM in a galaxy cluster, though this claim was disputed by Tsai (1994) using data from the other *Einstein* detectors with lower energy resolution.

White et al (1991) discovered intrinsic absorption in the *Einstein* SSS data of M87 which was later confirmed with *ASCA* (Allen et al, 2000). In these studies the absorber is assumed to be cold gas with solar abundances similar to the intervening cold gas in the Milky Way. The useful bandpasses of the *Einstein* SSS and *ASCA* SIS extend down to ~ 0.5 keV, and thus the *ROSAT* PSPC whose bandpass extends down to 0.1 keV should be even more sensitive to soft X-ray absorption from cold gas (or dust).

However, in the first detailed spectral analysis of the PSPC data of M87 Nulsen & Böhringer (1995) mention in passing that when the hydrogen column density is treated as a free parameter they obtain values *less* than Galactic. Although not emphasized by Nulsen & Böhringer (1995) this result is inconsistent with significant absorption from cold gas. A later *ROSAT* analysis by Allen & Fabian (1997) restricted consideration only to energies above 0.4 keV and also finds no evidence for absorption from cold gas in the PSPC data of M87. But a subsequent re-analysis by these authors now finds evidence for such absorption (Sanders, Fabian, & Allen 2000). The confused status of intrinsic X-ray absorption and multiphase gas in M87 warrants re-examination.

¹Chandra Fellow

The possible connection between the cooling flow and AGN in M87 has also received considerable attention recently. It has been known for some time (e.g., Böhringer 1997) that the X-ray isophotes are somewhat distorted within ~ 30 kpc of the center of M87, and these distortions appear to correlate with the radio emission. A new deep radio image obtained by Owen et al (2000) shows that the radio emission fills the central ~ 30 kpc region. The spatial correlation between radio and X-ray emission in M87 has been interpreted as evidence that the AGN has refashioned the hot ISM and stifled the cooling flow in the central region (Binney, 1999).

Therefore, we re-analyze the PSPC data primarily to search for oxygen absorption and warm gas in M87 similar to that found for the lower S/N galaxies and groups in PAPER1 and PAPER3. We also investigate cooling flow models in an attempt to clarify the possible connection between the AGN and cooling flow. The paper is organized as follows. In §2 we present the observations and discuss the data reduction. The deprojection procedure is summarized in §3. We discuss the spectral fitting of single-phase models in §4 and of multiphase models in §5. In §6 we discuss the results and in §7 we present our conclusions.

2. OBSERVATIONS AND DATA PREPARATION

We obtained the *ROSAT* PSPC data of M87 from the public data archive maintained by the High Energy Astrophysics Science Archive Research Center (HEASARC). The properties of the observations are listed in Table 1. The three observations have essentially identical exposures and pointings (i.e., centered on M87). Each observation was reduced separately, and we refer the reader to Buote (2000c, hereafter PAPER2) for details of our implementation of the standard data reduction procedures.

2.1. *Background Estimation*

Background spectra were obtained from source-free regions near the edge of the PSPC fields; i.e., $\sim 50'$ from the field centers. The principal advantage of a local background estimate is that residual contamination from solar X-rays and any other long-term background enhancements (Snowden et al, 1994) are fully accounted for in the ensuing spectral analysis. The disadvantage is that the extended X-ray emission of M87 and the Virgo cluster fills the entire PSPC field and must be disentangled from the true background. (Note that the background cluster emission is accounted for in the deprojection analysis – see §3.1 of PAPER2.)

We extracted the background spectra separately from each observation and then added them together. Since each observation occurred after the October 1991 gain change the Redistribution Matrix File (RMF), which specifies the channel probability distribution for a photon, is the same for each. Since, however, the detector location of background regions are in general slightly different for the different observations because of slight aspect differences, we averaged their respective Auxiliary Response Files (ARFs) which contain the information on the effective area as a function of energy and detector location.

To obtain an estimate of the true background we follow the procedure outlined in PAPER2 and fit the composite background spectrum with a model after subtracting the particle background. We represent the cosmic X-ray back-

ground by a power law with photon index $\Gamma = 1.4$ and the Galactic emission by two soft thermal components following Chen et al (1997). (Actually, for M87 we find that only one of these soft thermal components is required with a temperature ≈ 0.15 keV.) To account for emission from the extended cluster emission we include another thermal component with variable temperature. Each component is modified by the Galactic hydrogen column density listed in Table 1.

This composite model provides a good fit to the background spectrum ($\chi^2 = 193$ for 185 dof), and the additional thermal component representing the cluster emission is clearly required by the data; i.e., $\chi^2 = 352$ for 181 dof without the cluster component. The temperature of the cluster component is $1.5^{+0.4}_{-0.2}$ keV (90% confidence) which is somewhat less than the ~ 3 keV temperature inferred by Nulsen & Böhringer (1995) over the same regions of the PSPC data. These differences are probably the result of the different models used to compute the background. If, for example, we do not include the cosmic power law component in our fits then we obtain a temperature of ≈ 2.5 keV similar to Nulsen & Böhringer (1995). (Note that the temperature of the cluster component is very insensitive to the metallicity.)

Since the diffuse background is most important in the softest energy channels the stability of the background estimate to various assumptions can be assessed by considering the background flux between 0.2 and 0.3 keV. (The need for the 0.2 keV lower limit arises from PSF considerations – see below in §2.2.) Let us compare the 0.2-0.3 keV flux obtained from our best-fitting background model to a similar model where instead the cluster component temperature is fixed at 3 keV. We find that the 0.2-0.3 keV fluxes of the background models (after excluding the cluster components) differ by only 14% with the best-fitting model having the slightly larger 0.2-0.3 keV flux. (We also prefer the slightly larger background estimate from the best-fitting model as it allows a more conservative assessment of any intrinsic soft emission in M87.) The background rate of the best-fitting model (i.e., after excluding the 1.4 keV cluster component) is 1.5×10^{-3} cts s $^{-1}$ arcmin $^{-2}$ (Table 2) which is very similar to the value of $\approx 1.0 \times 10^{-3}$ cts s $^{-1}$ arcmin $^{-2}$ obtained for PSPC observations of three other Virgo galaxies in PAPER2.

We subtract the background spectrum from each source annulus (see below) following the procedure described in §4.1.4 (equation 1) in PAPER2. That is, the background model (cosmic+Galactic) is scaled to the source annulus accounting for differences in area, exposure, vignetting, and detector response between the source and background regions. The ambient Virgo emission is accounted for downstream in the deprojection analysis discussed in §3 (see also §3.1 of PAPER2).

2.2. *Source Spectra*

Since our interest lies principally in the central regions where any intrinsic oxygen absorption is expected to be most pronounced, we confine our analysis of the X-ray emission of M87 to the region within the central ring of the PSPC (radius 20'). This is also the best calibrated region of the PSPC and is not affected by shading by the radial spokes of the PSPC support structure.

TABLE 1
ROSAT PSPC OBSERVATIONS OF M87

z	N_{H} (10^{20} cm $^{-2}$)	Sequence No	Date (Mo/yr)	Exposure (ks)	Total Source Flux (ct s $^{-1}$)	Source Flux (erg cm $^{-2}$ s $^{-1}$)	Background (ct s $^{-1}$ arcmin $^{-2}$)
0.00430	1.8-2.0	rp800187n00	6/92	10.1/9.4	25.3	3.0×10^{-10}	1.5E-3
		rp800365n00	7/92	9.9/9.5			
		rp800365a01	12/92	10.0/9.7			

NOTE.—Galactic Hydrogen column density (N_{H}) is taken from Lieu et al (1996). The Exposure column lists first the raw exposure time and second the final filtered exposure. The total source count flux is computed within a radius of 18.8' or 98 kpc assuming $D = 18$ Mpc; i.e., within the PSPC central ring. Both the source flux and background count rate are evaluated over 0.2-2.2 keV.

The source spectra were extracted in concentric circular annuli located at the X-ray centroid (computed within a 2' radius) such that for each annulus the width was $\geq 1'$ and the background-subtracted counts was larger than some value (≈ 70000) chosen to minimize uncertainties on the spectral parameters for each system while maintaining as many annuli as possible. Data with energies ≤ 0.2 keV were excluded to insure that the PSF was $< 1'$ FWHM. For our on-axis sources $\sim 99\%$ of the PSF at 0.2 keV is contained within $R = 1'$ (Hasinger et al, 1995). Any background sources that were identified by visual examination of the image were masked out before the extraction.

3. DEPROJECTION METHOD

To obtain the three-dimensional properties of the X-ray emitting gas we deproject the data assuming spherical symmetry using the “onion-peeling” technique pioneered by Fabian et al (1981). That is, one begins by determining the emission in the bounding annulus and then works inwards by subtracting off the contributions from the outer annuli. A full account of our implementation of this procedure is given in PAPER2.

Since we confine our analysis to the region within the central ring of the PSPC there exists significant emission from M87/Virgo outside of the chosen bounding analysis. This constitutes a “cluster background” component that needs to be subtracted from each source annulus in addition to the cosmic+Galactic background discussed in §2.1. Following §3.1 of PAPER2 we represent the spatial distribution of this cluster background by a β -model with the same spectrum as the bounding annulus. (X-ray emissivity of a β model is $\propto r^{-6\beta}$ at large radius.) As in PAPER2 we find that the derived temperatures, abundances, and column densities are very insensitive to typical values of β for galaxies and clusters and thus we employ $\beta = 2/3$ for all results presented in §4 and §5.

We find that the radial profiles of the temperatures, Fe abundances, and column densities are generally well behaved. Hence, unlike for the galaxies and groups analyzed in PAPER2 we do not perform the quasi-regularization of the temperatures and abundances described in §3.3 of PAPER2. The greater stability of parameter values can be attributed to the much larger S/N of the M87 data.

(We mention that the deprojection procedure is invalid if there are gaps between annuli. This is another reason why we confined our analysis within the central ring of the PSPC.)

4. SINGLE-PHASE ANALYSIS

We initially focus our analysis on “single-phase” models of the hot gas; i.e., a single value for the temperature and density describes the emission of hot plasma at each radius. This is the simplest case and would seem *a priori* to be most appropriate for the low energy resolution of the ROSAT data. Below in §5 we consider multiphase models. As in previous studies we use the MEKAL plasma code (Mewe, Gronenschild, & van den Oord 1985; Kaastra & Mewe 1993; Liedahl, Osterheld, & Goldstein 1995) to represent the emission of hot gas at a single temperature.

We take the solar abundances in XSPEC to be those given by the Feldman (1992) table, because it contains the correct value of the solar Fe abundance, $\text{Fe/H} = 3.24 \times 10^{-5}$ by number. The popular table of Anders & Grevesse (1989) used in XSPEC has an old value for Fe/H which is too large by a factor of 1.44 as initially pointed out by Ishimaru & Arimoto (1997). See §4.1.3 of PAPER2 for further discussion.

According to the recent deconvolution analysis of ASCA data by White (2000) the Fe abundance of M87 is $\sim 0.9Z_{\odot}$ within the central arcminute, remains essentially constant at $\sim 0.6Z_{\odot}$ out to $\sim 9'$, and then falls to an average value of $\sim 0.4Z_{\odot}$ between $\sim 9' - 19'$ (all abundances scaled to meteoritic solar). These results agree with the multi-temperature models of the ASCA SIS data obtained by fitting the integrated spectra within 6' of M87 by Buote et al (1999). Consequently, when we fix the Fe abundance in selected models we assign it the value of $0.78Z_{\odot}$ appropriate for the two-temperature model of Buote et al (1999).

Following standard practice we represent the soft X-ray absorption arising from the Milky Way by cold material with solar abundances distributed as a foreground screen at zero redshift. In this standard absorption model the X-ray flux is diminished according to $A(E) = \exp(-N_{\text{H}}\sigma(E))$, where N_{H} is the hydrogen column density and $\sigma(E)$ is the energy-dependent photo-electric absorption cross section for a cold absorber with solar abundances.

Lieu et al (1996) have shown that the Galactic column density varies over the PSPC field of M87. Inspection of their Figure 2 reveals that $N_{\text{H}}^{\text{Gal}}$ varies almost radially outward from M87 taking a minimum value of 1.8×10^{20} cm $^{-2}$ near the center and a value of 2.0×10^{20} cm $^{-2}$ near our bounding annulus (#10). Since intermediate values of $N_{\text{H}}^{\text{Gal}}$ appear to prevail at intermediate radii we set $N_{\text{H}}^{\text{Gal}} = 1.9 \times 10^{20}$ cm $^{-2}$ in those cases where we fix $N_{\text{H}}^{\text{Gal}}$ in our models. In other instances we allow N_{H} to be a

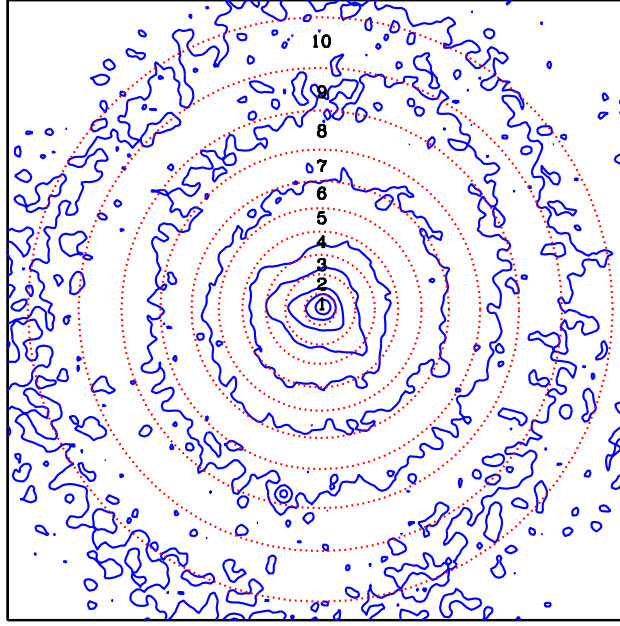


FIG. 1.— Contour plot of the ROSAT PSPC image (0.4 - 2.0 keV) of M87 corresponding to observation rp800187n00 (see Table 1). For display only the image was binned into $15'' \times 15''$ pixels and smoothed with a gaussian filter ($\sigma = 1$ pixel). The dotted (red) circles demarcate the source extraction annuli (see §2.2) defined as follows in units of arcminutes: annulus #1 0-1, #2 1-2.25, #3 2.25-3.5, #4 3.5-5, #5 5-6.5, #6 6.5-8.25, #7 8.25-10.25, #8 10.25-12.75, #9 12.75-15.5, and #10 15.5-18.75

TABLE 2
QUALITY OF SPECTRAL FITS (χ^2/DOF) FOR SINGLE-PHASE MODELS

Annulus	0NH_0Fe	1NH_0Fe	0NH_1Fe	1NH_1Fe	0NH_0Fe_E	1NH_0Fe_E	0NH_1Fe_E	1NH_1Fe_E
1	1678.0/186	583.8/185	1254.1/185	507.1/184	821.4/184	333.2/183	332.2/183	323.4/182
2	1056.1/189	784.0/188	1019.2/188	469.3/187	292.6/187	288.6/186	287.6/186	278.9/185
3	1097.2/190	647.1/189	1027.1/189	437.6/188	354.2/188	301.6/187	293.3/187	280.4/186
4	1248.4/190	617.8/189	1088.9/189	473.0/188	341.9/188	302.2/187	268.2/187	246.6/186
5	1355.6/190	567.7/189	1008.7/189	536.2/188	568.2/188	419.4/187	338.5/187	303.9/186
6	1358.7/190	424.2/189	909.8/189	397.9/188	509.8/188	307.7/187	242.2/187	222.7/186
7	1429.9/190	514.5/189	966.0/189	498.8/188	512.0/188	388.8/187	280.8/187	237.4/186
8	1383.7/190	420.4/189	860.0/189	415.4/188	375.3/188	346.8/187	251.0/187	227.6/186
9	1220.5/189	386.5/188	743.4/188	386.2/187	413.5/187	343.3/186	252.5/186	228.7/185
10	649.0/190	263.6/189	466.2/189	255.0/188	464.6/188	213.9/187	173.5/187	164.6/186

NOTE.—Models are labeled according to whether N_{H} (standard absorber) and/or the Fe abundance are free parameters in the fits. A “0” indicates the parameter is fixed and “1” indicates the parameter is variable. Models with “E” have an intrinsic oxygen absorption edge.

free parameter in our fits to indicate any excess absorption intrinsic to a galaxy or group and also to allow for any errors in the assumed Galactic value and for any calibration uncertainties. Note that in this standard model N_{H} is measured as a function of two-dimensional radius, R , on the sky in contrast to the emission parameters (e.g., gas temperature, Fe abundance) that are measured as a function of three-dimensional radius, r .

The photo-electric absorption cross sections used in this paper are given by Balucińska-Church & McCammon (1992). It has been pointed out by Arabadjis & Bregman (1999) that the He cross section at 0.15 keV is in error by 13% in the Balucińska-Church & McCammon (1992) compilation. Recently a new version of xSPEC (v11) has been released which updates the Balucińska-Church & McCammon (1992) table to include the more accurate He cross

sections of Yan et al (1998). We find that when using these more accurate He cross sections we obtain hydrogen column densities that are 5%-10% larger than when using the original Balucińska-Church & McCammon (1992) He cross sections in xSPEC v10. Where appropriate we mention these small differences below.

4.1. Standard Absorber

We begin with the model having the least number of free parameters. This corresponds to setting $N_{\text{H}} = N_{\text{H}}^{\text{Gal}}$ for the standard absorber and holding the Fe abundance fixed to $0.78Z_{\odot}$ as discussed above. The values of χ^2 for this model (0NH_0Fe) are listed in Table 2, and the spectral fits for the inner and outer annuli are displayed in Figure 2. It is clear from the large reduced χ^2 values and the large residuals in the spectral plots that this model provides a

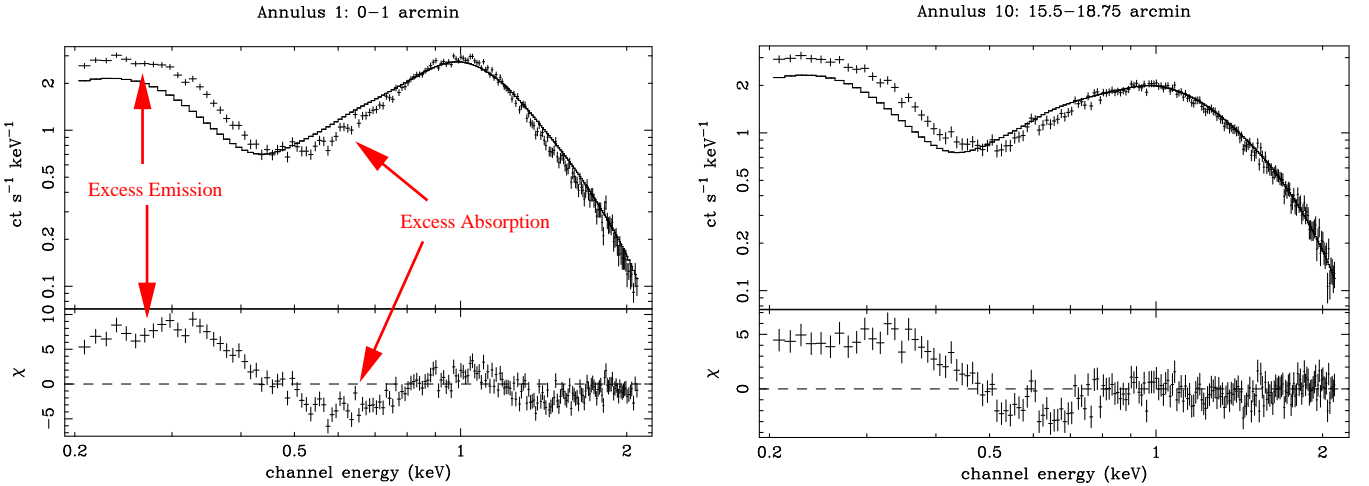


FIG. 2.— ROSAT PSPC spectra of the (Left) inner annulus and the (Right) outer annulus. The fitted models have hydrogen column density fixed to Galactic and Fe abundance fixed to $0.78Z_{\odot}$; i.e., model 0NH_0Fe of Table 1.

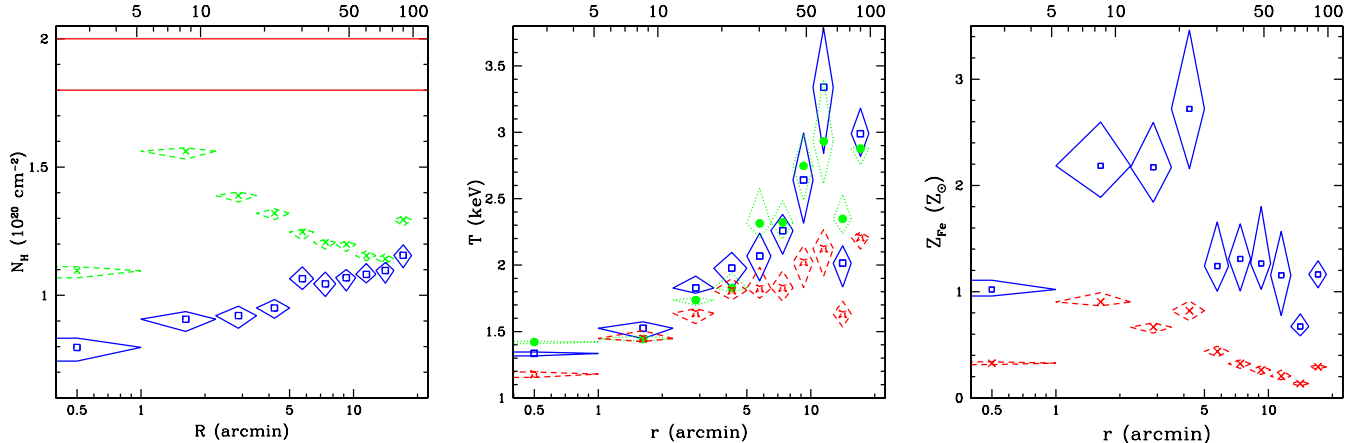


FIG. 3.— Fitted model parameters for selected single-phase models of Table 1 as a function of radius (units – bottom: arcminutes, top: kpc): (Left) Hydrogen column density profile of standard absorber for model 1NH_1Fe denoted by (blue) boxes for best-fitting values and (blue) solid diamonds for 68% error bars. Also shown is model 1NH_0Fe denoted by (green) crosses and dashed diamonds. The solid lines (red) indicate the range of Galactic column density: (Middle) Temperature profiles of models 1NH_1Fe (boxes/solid diamonds/blue), 0NH_1Fe (crossed/dashed diamonds/red), and 1NH_0Fe (circles/dotted diamonds/green); (Right) Fe abundance profiles for models 1NH_1Fe (boxes/solid diamonds/blue) and 0NH_1Fe (crossed/dashed diamonds/red).

very poor fit to the ROSAT PSPC spectra of M87.

Two regions of the spectra are primarily responsible for the poor fits. In the energy band 0.2-0.4 keV the data clearly lie above the model prediction. Immediately one can conclude that there is no intrinsic absorption from cold gas² for which we would have expected to see a deficiency of flux below the models with $N_{\text{H}} = N_{\text{H}}^{\text{Gal}}$. Instead soft emission in excess of this model is suggested. In contrast, between 0.5-0.8 keV the data do lie below the model consistent with intrinsic absorption. From inspection of Figure 2 the absorption appears to be more pronounced in the inner annulus.

These excess absorption and emission features are much too large to be explained by calibration error. The most significant calibration problem ever reported for the gain of the PSPC is by Snowden et al (1995) who showed that the early versions of the software to convert PHA (Pulse Height Analyzer) to PI (Pulse Invariant) channels did not

account for a gain deficit within a few arcminutes distance of the field center. This old problem only appeared in PI channels below 20 (i.e., below 0.2 keV) and is now almost entirely removed with the most up-to-date software which we have used. In principle such an uncorrected gain deficit would appear as an absorption feature in our analysis below 0.2 keV which is clearly unrelated to both the excess emission between 0.2-0.4 keV and the absorption between 0.5-0.8 keV observed in Figure 2. Further testament to the reality of these features is that they are each manifested over an energy range comparable to the PSPC resolution [$\Delta E/E = 0.43(E/0.93\text{keV})^{-0.5}$]; i.e., in the notation of Snowden et al (1994), who define resolved PSPC energy bands, the 0.2-0.4 keV interval is essentially the R2 band while 0.5-0.8 keV is essentially the R4 and R5 bands.

Although it might be tempting to equate the soft excess in the 0.2-0.4 keV band with an error in the background subtraction, this cannot be the case. The emission of the

²These results also apply for absorber models with partial covering factor $f = 0.5$ precisely as found for the galaxies and groups in PAPER3; see section 2.1 of PAPER1 and section 3.2 of PAPER3 for details. Since we find that the results obtained when using absorber models with partial covering are essentially identical to those obtained for the standard uniform-screen absorber, we only discuss the uniform screen.

diffuse background in the *ROSAT* band does peak at these low energies (e.g., Chen et al. 1997) and the temperature of gas required to explain the soft excess is consistent with the diffuse background (see below in §5.2). However, the background contributes only 0.6% of the 0.2-0.4 flux within the inner annulus, and thus only an (impossible) error of over two orders of magnitude in the background level could account for the excess 0.2-0.4 keV flux. Only for the bounding annulus (i.e., annulus #10) is a relatively small background error required (factor of ≈ 1.6) to explain the excess soft emission. But we have taken care to account for detector response differences between background and source positions (§2.1). The statistical error on the background is $\sim 1\%$ and we estimate at most a 15% systematic error in the background level arising if we do not subtract the “additional thermal component” attributed to M87 (§2.1). Hence, errors in the background subtraction cannot explain the excess 0.2-0.4 keV emission.

Since the deviations from the 0NH_0Fe model displayed in Figure 2 must be intrinsic to M87, let us now examine whether adjusting the available model parameters can improve the fits. If N_{H} is allowed to vary in the fits while keeping the Fe abundance, Z_{Fe} , fixed (i.e., model 1NH_0Fe in Table 2) then we obtain large improvements in the fits in all annuli; the least amount of improvement is observed for annuli #2-3. Although allowing N_{H} to vary removes a large portion of the deviations over 0.2-0.4 keV the absorption feature over 0.5-0.8 keV remains essentially unaffected.

The fitted values of $N_{\text{H}}(R)$ (see Figure 3) are $\approx 0.6N_{\text{H}}^{\text{Gal}}$ in most annuli with a maximum of $\approx 0.8N_{\text{H}}^{\text{Gal}}$ in annulus #2. These values are still very significantly less than the Galactic value when considering the 5%-10% underestimates arising from inaccuracies in the He cross sections (see immediately before §4.1). These sub-Galactic columns are also unaffected by possible errors in the plasma emission code (MEKAL). Since the fitted temperatures are always above 1 keV inaccuracies in the plasma code near energies 0.2-0.4 keV are negligible because at these temperatures the continuum dominates any neglected line emission which is the principal source of error (e.g., Liedahl 1999).

If instead Z_{Fe} is allowed to vary but N_{H} is held fixed at $N_{\text{H}}^{\text{Gal}}$ (i.e., model 0NH_1Fe in Table 2), then the fits are also improved though not quite so much as when N_{H} is allowed to vary. The improvement in the fits is again confined to the lower energies (0.2-0.4 keV) leaving the absorption deviations over 0.5-0.8 keV uncorrected. The sub-solar values of $Z_{\text{Fe}}(r)$ (Figure 3) are consistent with those obtained from the previous *ASCA* studies of White (2000) and Buote et al (1999). The *ASCA* measurements of Z_{Fe} should be more reliable since they are determined primarily by the 6.5 keV Fe K α line complex in contrast to the *ROSAT* determinations using the ~ 1 keV Fe L lines.

The temperature measurements from *ASCA* and *SAX* are also more reliable than those from *ROSAT* because of the much better energy resolution and the larger bandwidth. In Figure 3 one notices that for $r > 5'$ the model 0NH_1Fe has $T < 2.5$ keV which is very inconsistent with the temperatures obtained from *ASCA* (White, 2000) and *SAX* (D'Acri et al, 1998). On the other hand, if both N_{H} and Z_{Fe} are varied (i.e., model 1NH_1Fe in Table 2) then

$T(r)$ is consistent with *ASCA* and *SAX* but now Z_{Fe} is too large at all radii (Figure 3). This latter model also has fitted column densities that deviate from the Galactic value even more significantly than the 1NH_0Fe model discussed above. Interestingly, when both N_{H} and Z_{Fe} are varied significant improvement in the fits is also observed over 0.5-0.8 keV unlike when only one of these parameters is varied (though the overall fit quality is still poor in all annuli except #10).

Hence, the single-phase model with a standard absorber is demonstrably a very poor fit to the *ROSAT* data. Although improvements in the fits can be achieved by varying N_{H} and Z_{Fe} the resulting fits are still poor, the column densities are significantly below the Galactic value, and the fitted temperatures and abundances are not each consistent with the *ASCA* (and *SAX*) data for any particular model. We are thus compelled to conclude that a single-phase gas modified by a standard Galactic absorber cannot describe the X-ray data of M87.

4.2. Oxygen Edge

The striking residuals of excess absorption and emission apparent from visual inspection of the spectral fits of M87 (Figure 2) provide strong support for the analogous (but less obvious) properties deduced from the lower S/N data of the individual elliptical galaxies and galaxy groups studied in PAPER1 and PAPER3. An immediate result of critical importance is that since the data for energies below 0.5 keV do not lie below the 0NH_0Fe model in Figure 2, the low-energy PSPC data unequivocally rule out any significant excess absorption from cold absorbing matter which has frequently been advocated in the past for cooling flows. Instead, the absorption feature between 0.5-0.8 keV must arise from warm material as we have discussed extensively in PAPER1 and PAPER3.

Because of the low energy resolution of *ROSAT* it is instructive first to analyze the hydrogen column density obtained for the standard cold absorber as a function of the chosen lower energy limit (E_{min}) of the bandpass (see §3.3 of PAPER3). That is, we fitted the model 1NH_0Fe (defined above) to the PSPC spectrum including only data having energies between E_{min} and 2.2 keV. The results are displayed in Figure 4. When $E_{\text{min}} \approx 0.2 - 0.3$ keV the fitted column density is always similar to or less than $N_{\text{H}}^{\text{Gal}}$. As E_{min} increases to ~ 0.5 keV we find that $N_{\text{H}} \sim 1.5N_{\text{H}}^{\text{Gal}}$ for $R \gtrsim 5'$ and increases to $N_{\text{H}} \sim 3N_{\text{H}}^{\text{Gal}}$ for $R < 5'$. This radially decreasing profile of column density becomes even more pronounced for larger values of E_{min} ; e.g., as shown in Figure 4 for $E_{\text{min}} = 0.7$ keV the outer annuli have $N_{\text{H}} \approx N_{\text{H}}^{\text{Gal}}$ whereas at smaller radii $N_{\text{H}} = (3 - 6)N_{\text{H}}^{\text{Gal}}$. This trend continues up to $E_{\text{min}} \approx 0.8$ keV after which $N_{\text{H}}(R; E_{\text{min}}) \approx N_{\text{H}}(R; 0.8 \text{ keV})$ for $E_{\text{min}} > 0.8$ keV within the increasingly larger uncertainties.

In order to quantify the “warm” absorption and yet simultaneously fit the entire *ROSAT* spectrum we follow our previous investigations of galaxies and groups (PAPER1 and PAPER3) and model the intrinsic absorption with a single absorption edge represented as, $A(E) = \exp[-\tau(E/E_0)^{-3}]$ for $E \geq E_0$ where E_0 is the rest-frame energy of the edge and τ is the optical depth. Similar to the standard absorber we place the edge immediately in front of the source so τ is measured as a function of

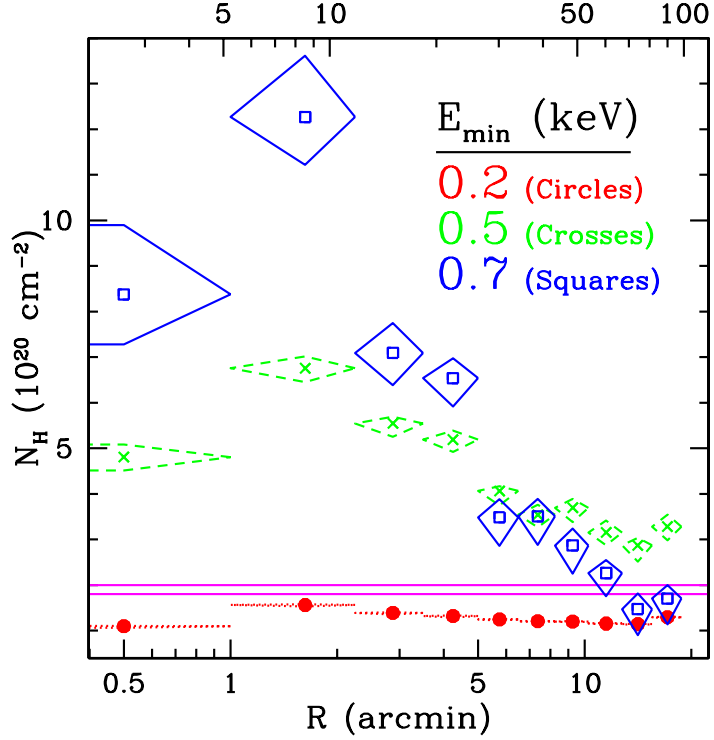


FIG. 4.— Radial profiles of hydrogen column density of the standard absorber for different values of the minimum energy of the bandpass (E_{\min}) corresponding to the single-phase model 1NH_0Fe using the notation of Table 2. Only data with energies $E > E_{\min}$ are included in the fits. The solid lines (magenta) indicate the range of Galactic column density.

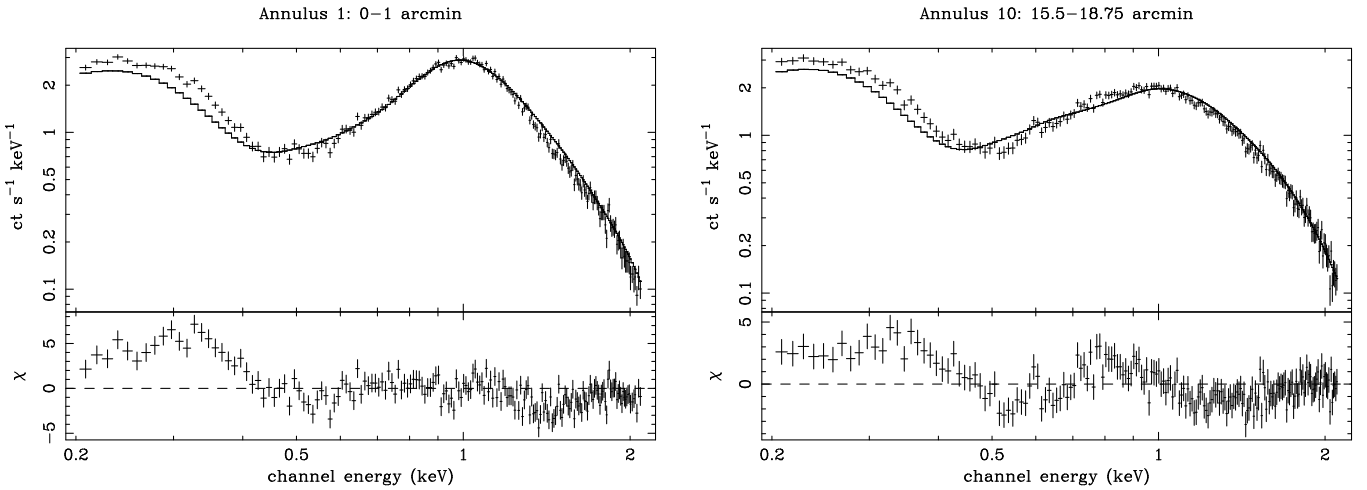


FIG. 5.— ROSAT PSPC spectra plotted as in Figure 2 except that now the model includes an intrinsic (oxygen) absorption edge; i.e., model 0NH_0Fe_E in Table 2.

2D radius R . A rigorous treatment of the warm absorber would (at least) include a series of absorption edges from different ionization states of principally oxygen but also of carbon and nitrogen similar to the models described by Krolik & Kallman (1984) that are currently not supported in XSPEC. Our simple parameterization of a warm absorber as a single edge is intended primarily as a phenomenological tool to establish the existence and to study the gross properties of the absorber which is appropriate for the low resolution data afforded by the PSPC.

We place the edge initially at $E_0 = 0.532$ keV appropriate for O I but always allow E_0 to vary; nevertheless we shall often refer to this as an “oxygen edge”. The values

of χ^2 for models with an oxygen edge are listed in Table 2, and in Figure 5 we plot the ROSAT spectra for annuli #1 and #10 in analogy to Figure 2 with the only difference being that the oxygen edge is included in the best-fitting models; i.e., model 0NH_0Fe_E.

Although the edge greatly improves the fits of all annuli, the character of the improvement varies with radius. As seen in Figure 5 for annulus #1 the oxygen edge removes most of the residuals over 0.5-0.8 keV while leaving other deviations (primarily at lower energies) mostly unchanged. This qualitative behavior also applies to the next few annuli (#2-4). In contrast, as seen for annulus #10 in Figure 5 the single oxygen edge itself is insufficient to

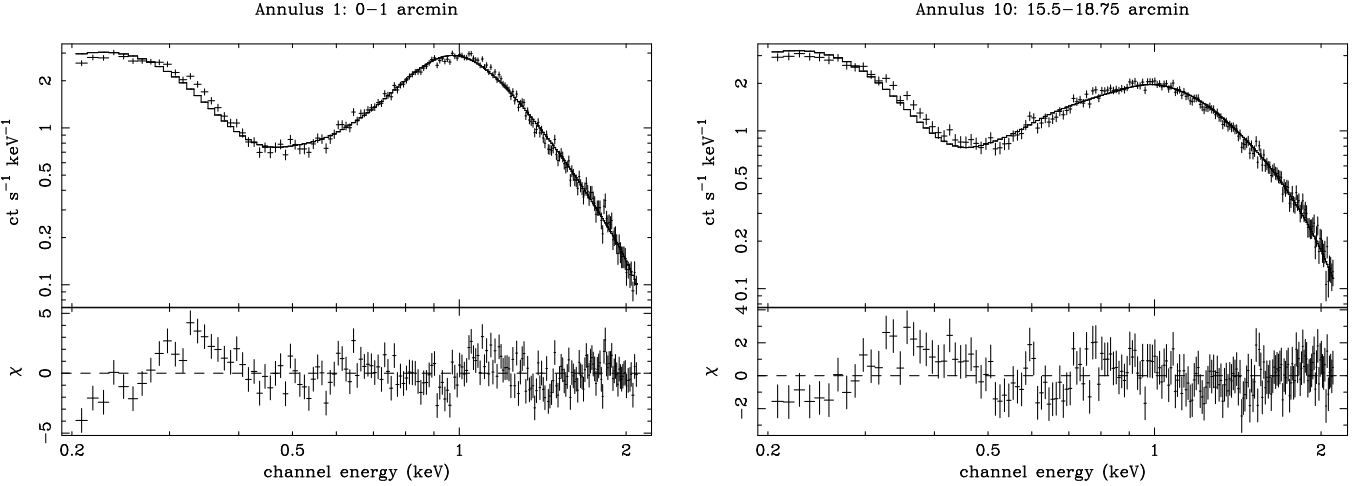


FIG. 6.— As Figure 5 except that now the model (with intrinsic absorption edge) also has variable hydrogen column density for the standard absorber; i.e., model 1NH_0Fe_E in Table 2.

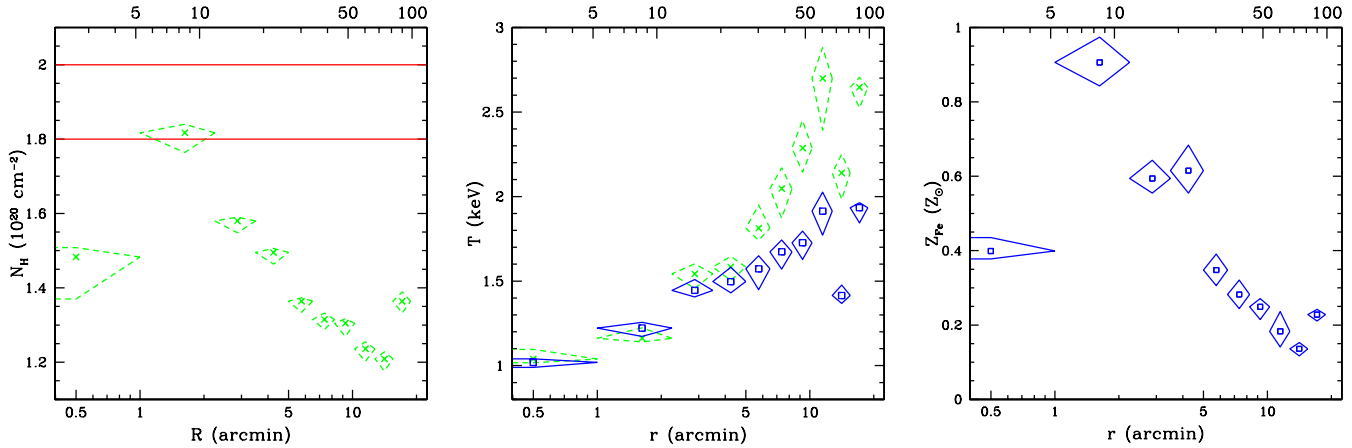


FIG. 7.— As Figure 3 except models now include an intrinsic oxygen edge: (Left) $N_H(R)$ for model 1NH_0Fe_E; (Middle) $T(r)$ for models 0NH_1Fe_E (crosses/dashed diamonds/green) and 0NH_1Fe_E (boxes/solid diamonds/blue); (Right) $Z_{Fe}(r)$ for model 0NH_1Fe_E.

remove the residuals over 0.5-0.8 keV and instead allows only a relatively crude improvement by cutting essentially midway through the 0.5-0.8 keV region; i.e., the model is still clearly the wrong shape in the absorbing region. This qualitative behavior applies to the outer annuli (#5-10).

When either N_H of the standard absorber or Z_{Fe} is allowed to vary the fits are improved substantially in most annuli; i.e., models 1NH_0Fe_E and 0NH_1Fe_E in Table 2. For annuli #1-4 the improvement offered by variable N_H and Z_{Fe} are very similar, and as seen in Figure 6 (using model 1NH_0Fe_E) most of the large residuals displayed by the original single-phase standard absorber model (Figure 2) have been removed.

The radial profiles of N_H , T , and Z_{Fe} for these edge models are displayed in Figure 7. For annuli #1-4 the temperatures are consistent for both models and the Fe abundance profile (for 0NH_1Fe_E) is essentially consistent with that obtained from the ASCA data (White, 2000) (scaled to meteoritic solar Fe abundance). The column density profile for the standard absorber is $\sim 20\%$ below the Galactic value for annuli #1,3-4. This discrepancy, though still statistically significant, is reduced to 10%-15% when using the more accurate He cross sections of (Yan et al, 1998) in XSPEC v11 (see immediately before §4.1). Note that if

both N_H and Z_{Fe} are varied (i.e., model 1NH_1Fe_E) the fitted parameters for annuli #1-4 are consistent with those above (though with larger errors) and the fits are slightly improved further (Table 2).

For the outer annuli (#5-10) although varying N_H improves the fits noticeably, a much larger improvement is obtained by varying Z_{Fe} . As can be seen in Figure 6 the variable N_H model (1NH_0Fe_E) fits the ROSAT spectrum for the bounding annulus (#10) quite well; the variable- Z_{Fe} model (0NH_1Fe_E) fits even better (Table 2). For annuli #5-9 the variable- Z_{Fe} model fits similarly to that shown for #10 except that the residuals below 0.5 keV are slightly more pronounced. If both N_H and Z_{Fe} are varied then the fits in these outer annuli are essentially formally acceptable (Table 2).

However, the fitted parameters obtained in these outer annuli indicate a problem with the simple single-phase, single-edge models. If Z_{Fe} is varied and N_H is held fixed then the inferred $Z_{Fe}(R)$ (Figure 7) is approximately consistent with the sub-solar values obtained by White (2000) for $R \gtrsim 5'$ with ASCA. But then the temperatures of this model are always below 2 keV at large R which are very inconsistent with the 2.5-3 keV temperatures inferred from ASCA and SAX (see discussion in §4.1). On the

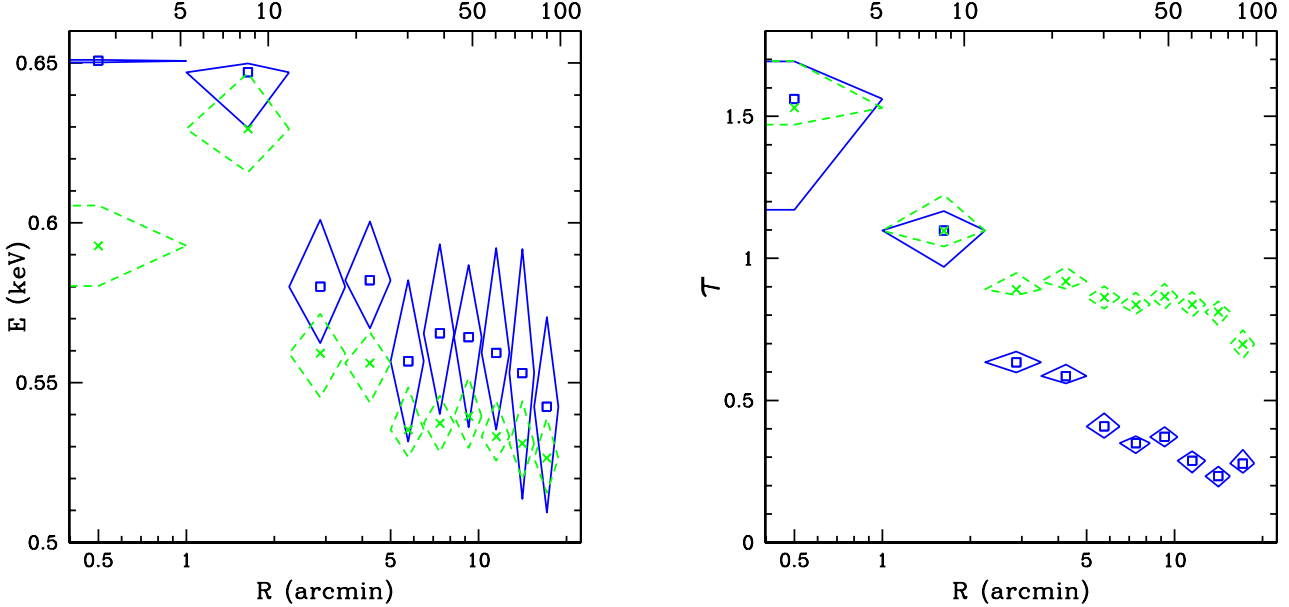


FIG. 8.— Intrinsic oxygen edge parameters for single-phase models: (Left) Oxygen edge energy, $E_0(R)$, for models 1NH_0Fe_E (crosses/dashed diamonds/green) and 0NH_1Fe_E (boxes/solid diamonds/blue); (Right) Oxygen edge optical depth, $\tau(R)$, for the same models.

other hand, if N_{H} is varied and Z_{Fe} is held fixed the fitted temperatures are consistent with *ASCA* /SAX but now $N_{\text{H}} \approx (0.6 - 0.7)N_{\text{H}}^{\text{Gal}}$ at large radius.

The lower temperatures inferred for 0NH_1Fe_E and the sub-Galactic columns inferred for 1NH_0Fe_E both imply the existence of an extra emission component having a temperature significantly less than the hot phase for annuli #5-10. For the inner radii #1-4 the temperatures are also consistently 30%-50% below the *ASCA* /SAX values (White 2000; D'Acri et al. 1998) and (except annulus #2) have sub-Galactic column densities which also suggest extra emission from cooler gas.

This cooler emission component is very likely related to the absorption component that we have modeled with the single oxygen edge. In Figure 8 we plot $E_0(R)$ and $\tau(R)$ for the models shown in Figure 7. For $R > 5'$, $E_0 \sim 0.55$ keV and then increases to $E_0 \sim 0.6 - 0.65$ keV at smaller R . Assuming collisionally ionized gas these edge energies imply a gas temperature ranging from $10^5 - 10^6$ K (e.g., Krolik & Kallman 1984; Sutherland & Dopita 1993) which apparently increases with decreasing R . The optical depth profile also falls with increasing R taking values near 1 for $R \lesssim 3'$ and flattens out for 1NH_0Fe_E or decreases steadily to values ~ 0.3 for 0NH_1Fe_E. Although $\tau(R)$ is quite similar to those obtained for the galaxies and groups studied in PAPER1 and PAPER3, the values of $E_0 \sim 0.6 - 0.65$ keV at small radii are significantly larger and probably indicate that the warm gas is “warmer” in M87.

Finally, we mention that attributing the 0.5-0.8 keV absorption feature instead to a sub-solar O/Fe ratio of the hot gas always results in sub-Galactic column densities for the standard absorber similar to that shown in Figure 2 for model 1NH_0Fe; i.e., sub-solar O/Fe still implies excess soft emission. And if this soft emission originates from ionized gas it should produce absorption near 0.5 keV. Moreover, sub-solar O/Fe models never fit as well as the

oxygen-edge models except when Z_{Fe} is held fixed and N_{H} is varied. In this case the sub-solar O/Fe models fit comparably to the oxygen-edge models at larger radius (annuli #5-10) but at smaller radii still have χ^2 values that are larger by 50-100. It should also be noted that these sub-solar O/Fe models all result in oxygen abundances that are zero everywhere which is in serious conflict with the theoretical expectation of approximately solar abundance ratios (e.g., Renzini et al. 1993). If O/Fe is kept to a minimum of $\sim 1/2$ solar then no sub-solar O/Fe model fits as well as a model with an oxygen edge. Hence, a sub-solar value for O/Fe of the hot gas cannot reasonably describe either the excess absorption over 0.5-0.8 keV or the excess soft emission over 0.2-0.4 keV.

(We also note that a very sub-solar value of O/Fe is inconsistent with the modest super-solar Si/Fe and S/Fe ratios measured by *ASCA* (e.g., Buote et al 1999); i.e., the α/Fe ratios should all give a consistent picture of the supernova enrichment.)

5. MULTIPHASE ANALYSIS

We have seen that an attempt to describe the *ROSAT* X-ray emission of M87 by a single-phase hot medium fails because the intrinsic absorption feature over 0.5-0.8 keV and the sub-Galactic hydrogen column densities (i.e., excess soft 0.2-0.4 keV emission) imply the existence of additional gas phases and cannot be explained by dust (§5.1 of PAPER3). In principle we would like to fit a general emission model in order to determine the differential emission measure function which fully characterizes the temperature structure of the plasma. Unfortunately, with detectors of low (*ROSAT*) and moderate (*ASCA*) energy resolution it is impossible to distinguish between different multiphase models. Buote et al (1999) showed in particular that two-phase models can easily mimic a multiphase cooling flow spectrum of galaxies and clusters. And in section 5.3 of Buote (1999) we showed that even with the

TABLE 3
QUALITY OF SPECTRAL FITS (χ^2/DOF) FOR MULTIPHASE MODELS

Annulus	Cooling Flow				Two Phases			
	0NH_0Fe_E	1NH_0Fe_E	0NH_1Fe_E	1NH_1Fe_E	0NH_0Fe	0NH_1Fe	0NH_0Fe_E	0NH_1Fe_E
1	329.2/183	324.9/182	325.7/182	320.1/181	529.8/184	389.3/183	288.1/182	256.2/181
2	299.0/186	295.0/185	289.0/185	276.5/184	746.5/188	370.3/186	288.9/185	229.4/184
3	312.0/187	308.2/186	295.7/186	275.7/185	597.0/188	375.5/187	283.7/186	244.0/185
4	290.9/187	294.0/186	270.6/186	238.7/185	564.3/188	404.5/187	261.0/186	236.9/185
5	424.1/187	372.2/186	335.0/186	298.2/185	527.0/188	489.0/187	321.1/186	295.8/185
6	365.4/187	286.3/186	247.5/186	230.4/185	384.0/188	353.2/187	240.1/186	227.6/185
7	422.6/187	330.6/186	267.6/186	232.5/185	473.6/188	452.9/187	257.3/186	242.0/185
8	415.3/187	299.2/186	242.3/186	223.2/185	384.9/188	377.9/187	231.8/186	215.3/185
9	413.0/186	303.3/185	247.9/185	226.6/184	360.5/187	359.1/186	240.5/185	225.3/184
10	259.8/187	180.7/186	160.4/186	156.7/185	248.4/188	241.7/187	203.7/186	150.3/185

NOTE.—The notation is as described in the notes to Table 2.

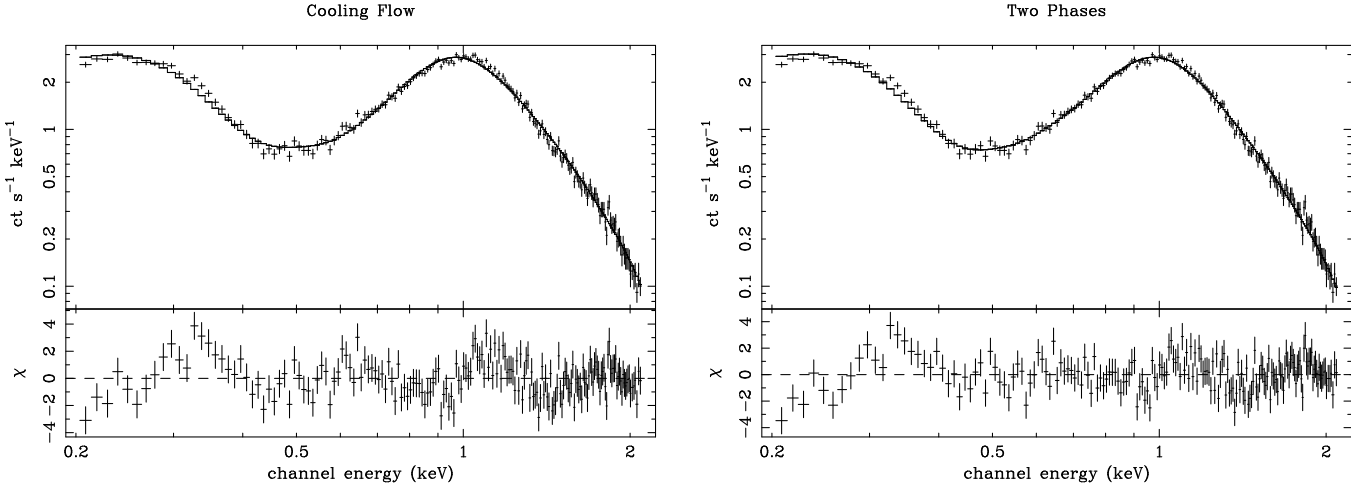


FIG. 9.— *ROSAT* PSPC spectrum of annulus #1 along with best-fitting models (0NH_0Fe_E) for (Left) a cooling flow and (Right) a two-phase medium.

higher resolution of ASCA the following multiphase models of galaxies all produced similar spectra: cooling flow, two-phase, and integrated single-phase temperature gradient; similar results were obtained for groups in Buote (2000a). (However, these very different multiphase models are each easily distinguished from isothermal models.)

Since the limited energy resolution of the PSPC prevents a detailed exploration of different multiphase models our primary objective in this section is to quantify the emission of the warm gas at each radius. As in our previous studies we examine the multiphase hypothesis in terms of the simple cases of a constant-pressure cooling flow and a two-phase medium. These models are instructive since they have been widely used to interpret the X-ray spectra of galaxies and clusters.

5.1. Cooling Flow

In the inhomogeneous cooling flow scenario the hot gas is expected to emit over a continuous range of temperatures in regions where the cooling time is less than the assumed age of the system. We consider a simple well-studied model of a cooling flow where the hot gas cools at constant pressure from some upper temperature, T_{\max} (e.g., Johnstone et al 1992). The differential emission measure of the cooling gas is proportional to $\dot{M}/\Lambda(T)$, where \dot{M} is the mass deposition rate of gas cooling out of the

flow, and $\Lambda(T)$ is the cooling function of the gas (in our case, the MEKAL plasma code).

Since the gas is assumed to be cooling from some upper temperature T_{\max} , the cooling flow model requires that there be a reservoir of hot gas emitting at temperature T_{\max} but is not cooling out of the flow. Consequently, our cooling flow model actually consists of two components, CF+1T, where “CF” is the emission from the cooling gas and “1T” is emission from the hot ambient gas. We set T_{\max} of the CF component equal to the temperature of the 1T component, and both components are modified by the same photoelectric absorption. Hence, the cooling flow model adds only one free parameter (\dot{M}) to those of the single-phase models.

If only absorption from the standard cold absorber model is considered then we obtain results identical to the single-phase models in §4.1; i.e., the CF component is completely suppressed by the fits. Since the CF model includes temperature components below ~ 0.5 keV it has stronger O VII (~ 0.56 keV) and O VIII (~ 0.65 keV) K α lines than the single-phase models which, as shown above, already predict too much emission from these lines. Therefore, in exact agreement with our *ROSAT* analysis of galaxies and groups in PAPER3 we find that only when an intrinsic oxygen absorption edge is included in the fits can we obtain a significant contribution from a CF component, and we shall henceforth restrict ourselves to cooling

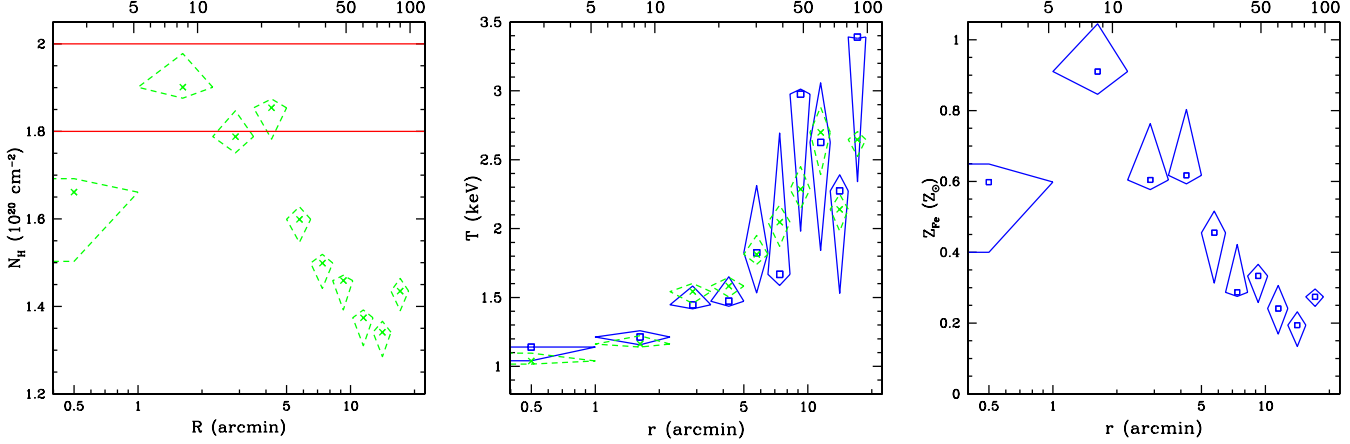


FIG. 10.— Same as Figure 3 except for cooling flow models. Model with fixed Z_{Fe} and variable N_{H} (1NH_0Fe_E) is denoted by crosses/dashed diamonds/green, and model with Galactic N_{H} and variable Z_{Fe} is denoted by boxes/solid diamonds/blue (0NH_1Fe_E). The temperature is associated with the ambient phase (i.e., T_{max}).

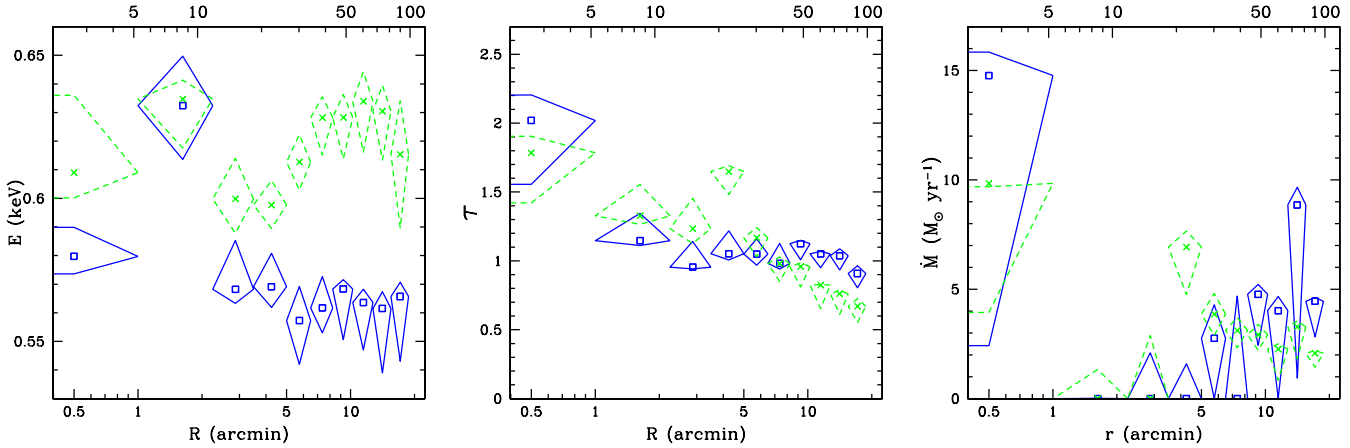


FIG. 11.— Intrinsic oxygen edge parameters for cooling flow models: (Left) Oxygen edge energy, $E_0(R)$, for models 1NH_0Fe_E (crosses/dashed diamonds/green) and 0NH_1Fe_E (boxes/solid diamonds/blue); (Right) Oxygen edge optical depth, $\tau(R)$, for same models.

flow models with an intrinsic oxygen edge.

The χ^2 values for selected cooling flow models with an intrinsic oxygen edge are listed in Table 3. Let us focus initially on the model 0NH_0Fe_E for comparison to the single-phase version. We plot 0NH_0Fe_E in Figure 9 for annulus #1 which should be compared to the single-phase version in Figure 5. The cooling flow model in the central annulus is a much better fit because it can mostly account for the soft emission over 0.2-0.4 keV. To a lesser extent the cooling flow model also provides a better fit in annuli #3-7 and 10, where the improved χ^2 values are intermediate with those obtained when varying N_{H} for the single-phase model (1NH_0Fe_E in Table 2). Thus, the cooling flow model is able to partially compensate for the excess soft emission. (This is also evident from $N_{\text{H}}(R)$ displayed for model 1NH_0Fe_E in Figure 10; i.e., for $R \lesssim 5'$ the fitted column densities are consistent with the Galactic value especially when considering the 5%-10% underestimates arising from the old He cross sections – see immediately before §4.1.)

If Z_{Fe} is allowed to vary then the quality of the resulting cooling flow model is very similar to the corresponding single-phase model (0NH_1Fe_E), though the cooling flow gives χ^2 values that are 5-10 lower in most annuli. The

temperature and Fe abundance profiles of the cooling flow model are shown in Figure 10. The Fe abundances are consistent with the single-phase model and the ASCA data (White, 2000). However, the temperatures of the cooling flow model at large radii are 2.5-3.0 keV which, unlike the single-phase model, are indeed consistent with the ASCA /SAX values; i.e., the cooling flow model 0NH_1Fe_E provides slightly better fits and physical temperatures and Fe abundances in the hot gas in contrast to the single-phase model.

The absorption parameters obtained for the cooling flow models are qualitatively similar to those obtained for the single-phase models (Figure 11). The $\tau(R)$ values for 0NH_1Fe_E are larger for the cooling flow model especially at large radii where $\tau \sim 1.0$ compared to $\tau \sim 0.3$ for the single-phase version. The larger optical depths for the cooling flow models are attributed to the need to suppress the stronger O VII and O VIII K α emission lines arising from the cooler temperature components.

Finally, in Figure 11 we also plot $\dot{M}(R)$ for the two cooling flow models. We see a strange profile where (apparently) there is significant cooling ($\dot{M} \sim 10 M_{\odot} \text{ yr}^{-1}$) at the center which abruptly terminates in annuli #2-4 and then rises to a nearly constant value ($\dot{M} \sim (3-4)$

$M_{\odot} \text{ yr}^{-1}$) at large radius. In the central bin the value of \dot{M} is uncertain and consistent with zero at the 90% confidence level and therefore is also consistent with the original *Einstein* value of $\dot{M} \sim 3 M_{\odot} \text{ yr}^{-1}$ (e.g., Canizares et al. 1982; Stewart et al. 1984). The total mass deposition rate of all annuli is $\dot{M} = 40^{+13}_{-31} M_{\odot} \text{ yr}^{-1}$ for model 0NH_1Fe_E and $\dot{M} = 34^{+8}_{-14} M_{\odot} \text{ yr}^{-1}$ for model 1NH_0Fe_E (1σ errors). These values of \dot{M} are in good agreement with the previous (imaging) *ROSAT* study by Peres (1998) and are also similar to the deposition rates of the brightest galaxy groups (Buote, 2000a) and small galaxy clusters. The implications of the mass deposition profile are discussed in §6.4.

5.2. Two Phases

The constant-pressure cooling flow model is one example of a (multiphase) gas that emits over a continuous range of temperatures, and it has the virtue of introducing only one free parameter (\dot{M}) to the single-phase models. A two-phase model, however, introduces two free parameters to the single-phase case: extra temperature and normalization. From our previous studies (e.g., Buote 1999, 2000a; Buote et al. 1999) we know that the two-phase model will fit as well or better than the cooling flow model, and the temperatures and Fe abundances will be similar in both cases. For our current purposes the two-phase model is useful since it allows us (1) to assign a specific temperature to the warm phase and (2) to explicitly quantify the relative contribution of the warm gas emission to the total.

We expect that adding the “warm” temperature component will have a similar effect as allowing N_{H} to vary in the fits of the single-phase models. For models without an intrinsic oxygen edge, it can be seen in Table 3 that the two-phase models 0NH_0Fe and 0NH_1Fe have very similar (actually somewhat better) χ^2 values than their single-phase counterparts with variable N_{H} (1NH_0Fe and 1NH_1Fe) in Table 2. The same behavior also applies to the corresponding two-phase models with an intrinsic oxygen edge (0NH_0Fe_E and 0NH_1Fe_E). The best-fitting two-phase model 0NH_0Fe_E for annulus #1 displayed in Figure 9 looks quite similar to the corresponding single-phase version with variable N_{H} (i.e., 1NH_0Fe_E) displayed in Figure 5.

The temperature profiles of the two-phase models are shown in Figure 12. The temperature of the warm gas (T_{w}) is essentially constant with radius with value 0.1 keV for the model without the oxygen edge. For the model with the oxygen edge $T_{\text{w}} \sim 0.2$ keV though it can be as large as 0.4 keV at intermediate radii. Although these temperatures are similar to that of the X-ray background, we recall that error in the background subtraction cannot account for the warm emission (§4.1). Note also that the value of T_{w} in annulus #2 is very uncertain because the warm emission there is weak, and thus we had to fix the value of T_{w} in annulus #2 to that of annulus #3. The temperature of the hot phase (T_{h}) in both cases is similar and is also very consistent with the 2.5-3 keV temperatures obtained by *ASCA* (White, 2000) and *SAX* (D’Acri et al. 1998) at large radii.

In Figure 12 we also show the fraction that the warm temperature component contributes to the total emission measure. Over most radii the warm temperature compo-

nent contributes 10%-20% to the emission measure. However, in annulus #2 the warm component is markedly suppressed and is consistent with zero for the model with an oxygen edge. The variation of emission-measure fraction with radius is qualitatively similar to the profile of \dot{M} for the cooling flow model (Figure 10); i.e., even though the cooling flow and two-phase models have entirely different differential emission measures they give essentially identical pictures of the variation of warm gas with radius.

The absorption parameters of the intrinsic oxygen edge for the two-phase model 0NH_0Fe_E are displayed in Figure 13. Both the rest energies of the edge and the optical depths are (nearly) consistent with being constant with radius. Although these flat profiles are somewhat different from the cooling flow and single-phase models, the ranges of values of energies and optical depths are similar.

6. DISCUSSION

6.1. Comparison with Previous X-Ray Studies of M87

Using a spatial-spectral deprojection analysis we have shown that a single-phase model of the hot gas modified by standard Galactic absorption cannot describe the *ROSAT* PSPC data of M87. The failure of the single-phase model is dramatically evident in the spectral plot in Figure 2: excess absorption over 0.5-0.8 keV and excess emission over 0.2-0.4 keV signal the presence of an additional warm ($\sim 10^6$ K) gas component. This evidence for warm absorbing (and emitting) gas in M87 lends strong support to the results we have recently obtained from *ROSAT* data of several bright galaxies and groups (PAPER1 and PAPER3).

Only multiphase models (e.g., cooling flow, two-phase) with an intrinsic oxygen edge are able to provide good fits to the *ROSAT* data and still have (1) ambient temperatures and Fe abundances consistent with *ASCA* and *SAX* studies (§4.1) and (2) Galactic hydrogen column densities for the known absorption arising from the intervening cold gas in the Milky Way. Although the multiphase models provide better fits than the single-phase models, they still do not provide perfect fits in all annuli (Figure 9). The remaining low-level residuals can be eliminated by allowing the α -process elements to vary differently from Fe; e.g., the most important element is Si which removes most of the residual if Si/Fe is allowed to be several times solar. A modest super-solar Si/Fe ratio is consistent with previous *ASCA* studies (Buote et al. 1999 and references therein). Since *ROSAT* is unable to place tight constraints on the abundance ratios we do not give constraints on these quantities at this time.

It is also possible that these low-level residuals in our best models reflect calibration errors. In particular, the remaining feature between near 0.3 keV (Figures 6 and 9) is very similar to that seen in the PSPC spectra of some other bright clusters in the recent study by Arabadjis & Bregman (2000). These authors prefer to explain these low-level residuals as a gain offset.

While preparing our manuscript we became aware of the preprint by Sanders et al (2000). These authors also present a spatial-spectral deprojection analysis of the *ROSAT* data of M87 along with a large sample of clusters. The analysis of Sanders et al (2000) differs from ours in two main respects. First, they bin up each PSPC spectrum

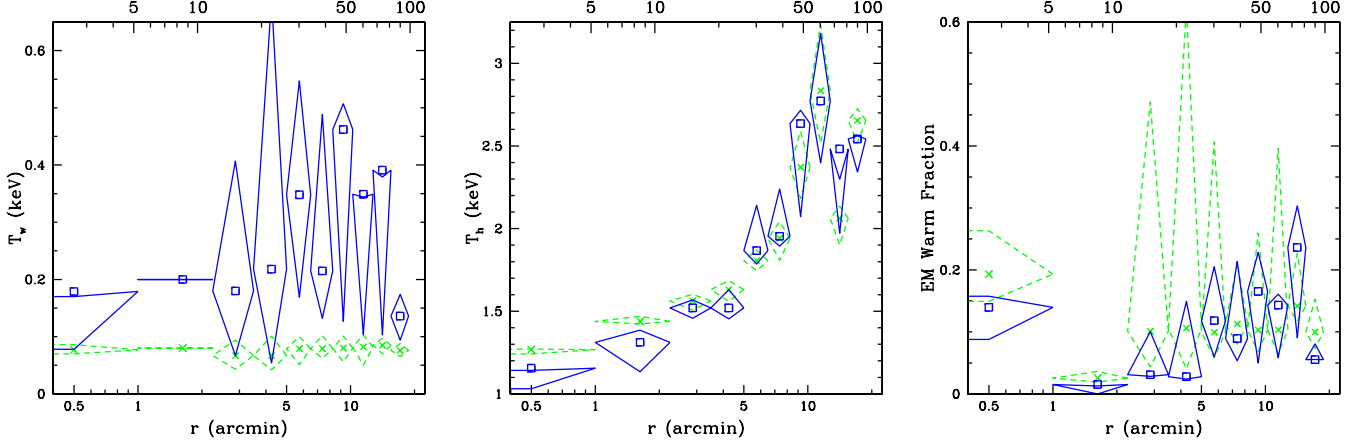


FIG. 12.— Temperatures for two-phase models without an intrinsic oxygen edge (0NH_0Fe in Table 3; crosses/dashed diamonds/green) and with the edge (0NH_0Fe_E in Table 3; boxes/solid diamonds/blue). The temperature for the warm component (T_w) is shown in the left panel and that of the hot component (T_h) is shown in the middle panel. The fraction that the warm component contributes to the total emission measure is shown in the right panel. Note in each model we fix T_w in annulus #2 to the value obtained in annulus #3 as discussed in the text.

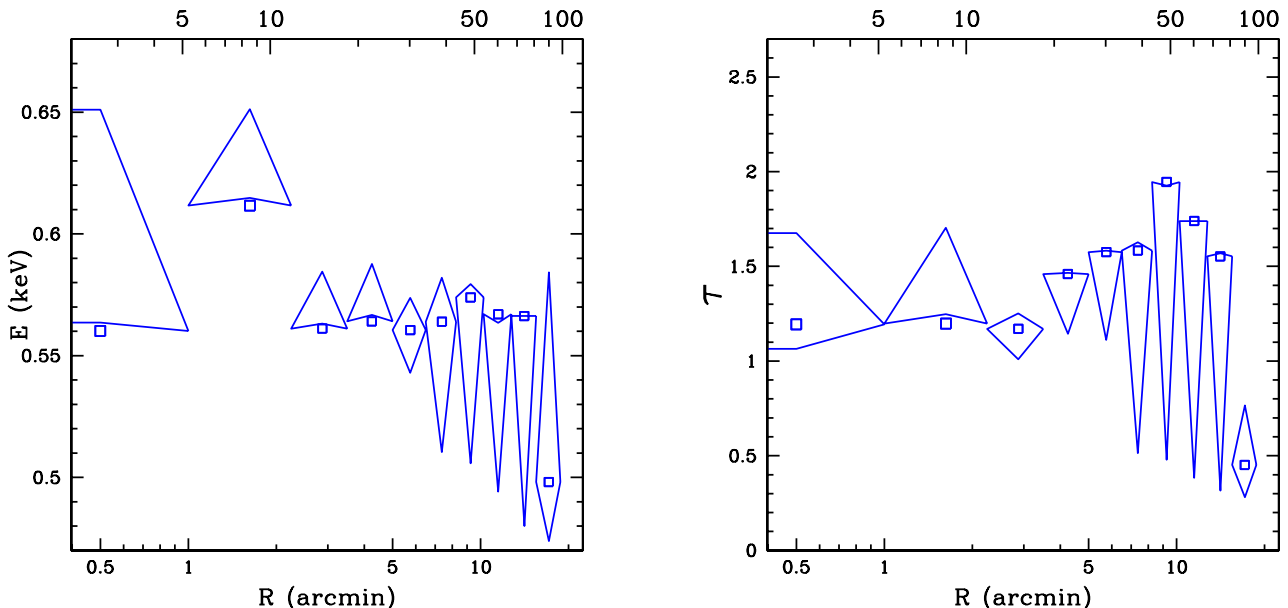


FIG. 13.— Properties of the intrinsic oxygen absorption edge for the two-phase model 0NH_0Fe_E: (Left) rest energy and (Right) optical depth.

into three X-ray channels (or “colors”). Spectral models are then fitted to ratios of these channels. Second, they exclude data below 0.4 keV and ignore the sensitivity of the inferred N_{H} to E_{min} shown in our Figure 4. Despite these differences between our respective analyses, Sanders et al (2000) also conclude that a single-phase model is inadequate and that spatially extended intrinsic absorbing material is required. Since, however, Sanders et al (2000) exclude data below 0.4 keV they do not detect the excess soft emission and thus are not led to conclude that the absorber must be warm.

Intrinsic absorption in M87 is also inferred from two-temperature models of the integrated ASCA spectra within $R \sim 5'$ by Allen et al (2000) which confirms the original detection with *Einstein* (White et al, 1991). The hydrogen column density of cold material implied by the two-temperature ASCA models, $(4 - 5) \times 10^{21} \text{ cm}^{-2}$, is considerably larger than the value of $1.4 \times 10^{21} \text{ cm}^{-2}$ ob-

tained by Sanders et al (2000) with *ROSAT* data. The smaller value obtained by Sanders et al (2000) arises from their fitting *ROSAT* data with energies above 0.4 keV with a cold absorber whereas the *ASCA* analysis of Allen et al (2000) includes only data above 0.6 keV. As we have shown in Figure 4 the inferred value of N_{H} is highly sensitive to the lower energy limit of the bandpass. Our absorption models using a single oxygen edge yield optical depths of ~ 1 in the inner regions of M87. These optical depths translate to $N_{\text{H}} = (3 - 4) \times 10^{21} \text{ cm}^{-2}$ (depending on the ionization state of oxygen) which agree with the *ASCA* result.

The new *ROSAT* evidence for multiphase gas in M87 largely confirms and extends the original detection by Canizares et al (1982) within the central $\sim 2'$ using the *Einstein* FPCS. By measuring selected line blends of Fe XVII - Fe XXIV Canizares et al (1982) inferred the presence of plasma emission components with temperatures

ranging from 3×10^7 K down to $2 - 4 \times 10^6$ K consistent with our results. However, these authors also deduce from analysis of the ly- α O VIII line that the O/Fe ratio is 3-5 times solar in the ISM (standard Galactic absorption was also assumed). Since this is not confirmed by either the *ROSAT* or *ASCA* data (which instead indicate that the data are absorbed over 0.5-0.8 keV where the ly- α O VIII line emits) the super-solar O/Fe ratio probably can be attributed to the FPCS calibration errors discussed by Tsai (1994) for M87.

An alternative explanation (due to the referee) for the FPCS measurement is as follows. Since the FPCS operated over a narrow energy band, if the absorption edges are confined to energies just below the O VIII K α line they would not be seen by the FPCS. Consequently, the FPCS would measure the line strength with respect to the absorbed continuum level. Lower resolution detectors like *ROSAT* and *ASCA* would merge the edge and line and therefore see a smaller line strength.

6.2. Mass of the Warm Gas

We now consider how much mass is associated with the warm ionized absorber in M87. In principle this can be computed from the optical depths of the intrinsic oxygen edges (Figures 8, 11, and 13), the mass deposition rates of the cooling flow models (Figure 11), or the emission measures of the warm gas in the two-phase models (Figure 12). Unfortunately, our single-edge absorption model is really just a phenomenological tool to establish the existence and to study the gross properties of the absorber which is appropriate for the low resolution of the PSPC (§4.2). As discussed in PAPER3, when including additional edges the inferred optical depth for each edge decreases, and we expect several edges from different ionization states of oxygen (also carbon and nitrogen) to contribute. Since the absorption of an edge is not linear in the energy of the edge (i.e., $A_0(E) = \exp[-\tau_0(E/E_0)^{-3}]$ and $A_1(E)A_2(E) \neq A_{1+2}(E)$ if the edge energies $E_1 \neq E_2$), by spreading multiple edges over a large energy range one can produce the observed absorption with smaller total optical depth than can be achieved with a single edge. Consequently, the single-edge optical depths should be considered upper limits.

Nevertheless, to provide a convenient benchmark for comparison to PAPER3 and to related previous studies, we have computed the absorber masses by assuming the absorption edges correspond to O I (see §5.3 of PAPER3). Using the single-phase model 1NH_0Fe_E as an example, we find that within the central bin (5 kpc) that the absorber mass is, $M_{\text{abs}} = 3.3_{-0.8}^{+0.3} \times 10^9 M_{\odot}$ (1σ errors) which is about twice that of the hot gas, $M_{\text{hot}} = 1.20_{-0.05}^{+0.01} \times 10^9 M_{\odot}$. The total values within 98 kpc are respectively, $M_{\text{abs}} = 2.4_{-0.3}^{+0.3} \times 10^{11} M_{\odot}$ and $M_{\text{hot}} = 2.14_{-0.04}^{+0.02} \times 10^{11} M_{\odot}$; i.e., $M_{\text{abs}} \approx M_{\text{hot}}$ similar to that found for the galaxies and groups in PAPER3. The amount of time required to accumulate M_{abs} assuming $\dot{M} = 40_{-31}^{+13} M_{\odot} \text{ yr}^{-1}$ (§5.1) is $t_{\text{acc}} = 0.6_{-0.2}^{+2.4} \times 10^{10} \text{ yr}^{-1}$; i.e., this absorbing material could reasonably have been accumulated by a cooling flow in agreement with the galaxies and groups in PAPER3.

If, as we expect, the absorber is the same material that gives rise to the excess 0.2-0.4 keV emission, then the above

values of M_{abs} should be (nearly) the same as M_{warm} ; i.e., the mass of the warm gas component of the two-phase models (§5.2). However, there are two key problems with translating the results of §5.2 into values of M_{warm} . First, the temperatures of the warm components are 0.1-0.2 keV, and it has recently been emphasized that the current plasma codes (including MEKAL) can underestimate the emission around 0.2 keV by as much as a factor of 10 at these low temperatures because of neglected line emission (Liedahl 1999; Beiersdorfer et al. 1999). Second, since the warm gas absorbs photons from the hot gas the assumption of collisional ionization equilibrium is also not strictly valid nor is it clear that the warm gas is fully optically thin to its own radiation as we have assumed for convenience (with MEKAL).

These problems are evident when we attempt to compare the emission measures ($\propto n_e^2 V$) of the warm gas component in the two-phase model to that implied by the values of M_{abs} quoted above from the oxygen edges. We find that, e.g., in the central radial bin the emission measure implied by the oxygen edges is ~ 30 times that inferred for the warm gas component in the two-phase model. This discrepancy is probably exacerbated by the “missing line” problem in the plasma codes, but can be mitigated by consideration of the following. First, by including multiple edges in our fits we can reduce the total optical depth by factors of a few leaving a factor of ~ 10 discrepancy. Second, if we consider the radiative transfer effects mentioned above (i.e., photoionization) then the warm gas is over-ionized for its (collisional) temperature. The inferred (collisional) emission measure is very sensitive to the temperature, and if we reduce the 0.1-0.2 keV temperature by a factor of ~ 3 the discrepancy of emission measures can be fully mitigated.

This exercise highlights the need for a more rigorous (and complex) treatment of the absorption and emission of the warm gas in order to deduce the mass of the absorber which is beyond the scope of our paper. If our basic results are confirmed with the substantially higher quality data from *Chandra* and *XMM*, then it will be appropriate to expend the effort to construct rigorous models of the warm absorber accounting for many edges and possible radiative transfer effects that are not currently available in XSPEC.

Finally, it is also worth mentioning that (these caveats aside) the emission from the warm gas implied by our measurements does not violate published constraints in the FUV similar to that found for the the galaxies and groups in section 5.4 of PAPER3. Dixon et al (1996) have reported results in the FUV for M87 obtained with the Hopkins Ultraviolet Telescope (HUT). They obtain a 2σ upper limit of $\sim 1 \times 10^{-10} \text{ erg cm}^{-2} \text{ s}^{-1}$ within $R = 1'$ of M87 for the flux of the O VI (1034Å) line which is expected to be the strongest line associated with warm gas having temperatures between 10^{5-6} K. Using M_{abs} quoted above we estimate that the strength of the O VI line at the peak temperature of 3.2×10^5 K (e.g., Pustinner & Sarazin 1994; Voit & Donahue 1995) is $\sim 9 \times 10^{-10} \text{ erg cm}^{-2} \text{ s}^{-1}$. Ignoring the fact that M_{abs} is over-estimated as discussed above, the HUT constraint implies that the T_w must be different from 3.2×10^5 K. From examination of Figure 7 of Voit & Donahue (1995) we see that the O VI luminosity decreases very rapidly with increasing temperature. Con-

sequently, the emission implied by M_{abs} is consistent with the HUT constraint provided that $T_w \gtrsim 5 \times 10^5$ K.

6.3. EUV Emission

Various conflicting reports of the detection of excess EUV (0.07-0.25 keV) emission above that expected from the hot (X-ray) plasma have been reported in clusters of galaxies using data from the *Extreme Ultraviolet Explorer* (*EUVE*), but only for M87 does there appear to be a consensus among different groups of the reality of centrally concentrated excess EUV emission (Lieu et al. 1996; Berghöfer et al. 2000). If the excess *EUVE* emission is interpreted as arising from optically thin collisionally ionized gas then Lieu et al (1996) and Berghöfer et al (2000) infer temperatures (~ 0.1 keV) and total masses within $R = 19'$ ($\sim 1 \times 10^{11} M_\odot$), which (considering the modeling differences between our studies) are in good agreement with those values we have inferred from the *ROSAT* data.

We mention that it has usually been reported that the *EUVE* “soft excess” of M87 increases with radius (e.g., Bonamente, Lieu, & Mittaz 2000). This result depends on the definition of the model of the hot gas that serves as the reference for the excess. The radially increasing soft excess assumes that the reference model for the hot gas has been fitted to the PSPC data using only data above 1 keV. If instead all the PSPC data are included in the fit, then there is no significant trend for the soft excess with radius in the *EUVE* data (R. Lieu 2000, private communication). This is consistent with our result for the two-phase models where the warm gas fraction is essentially constant for $R \gtrsim 5'$ (Figure 12).

Various problems with a gas origin of the EUV emission have been discussed by Fabian (1996), in particular the need for some as-yet-undiscovered heat source to prevent the gas from rapidly cooling to lower temperatures. These problems have spurred many to explain the excess EUV emission from other non-thermal processes (see Berghöfer et al. 2000 and references therein). However, an independent test of the hypothesis of warm ionized gas is offered by its absorbing effect on the hot X-ray plasma. Our detection of absorption confined to energies 0.5-0.8 keV is precisely the signature expected from warm (~ 0.1 keV) gas (e.g., Krolik & Kallman 1984).

The results from *EUVE*, *ROSAT*, and *ASCA* for M87 form a coherent picture of a multiphase medium consisting (approximately) of a warm and hot phase: The emission from the warm gas is detected with *EUVE* and *ROSAT* while the absorption from the warm gas is detected in *ROSAT* and *ASCA*.

6.4. Implications for Cooling Flows and AGN Feedback

The warm ($\sim 10^6$ K) gas we have detected in both absorption and emission with *ROSAT*, which is consistent with both the excess absorption seen in *ASCA* and the excess emission in *EUVE*, provides direct evidence for the material that may have cooled and dropped out of an inhomogeneous cooling flow (e.g., Fabian 1994). Although the warm gas is consistent with the amount of matter that could have been deposited by a cooling flow (§6.2), it is difficult to explain the warm gas phase as an equilibrium configuration because (1) the gas at $T \sim 10^6$ K cannot be thermally supported in the potential of M87, and (2) the

cooling time of this gas is very short (see section 5.5 of PAPER3).

Non-equilibrium models in the form of feedback from the central AGN have been proposed to largely suppress cooling flows (Binney & Tabor 1995; Ciotti & Ostriker 2000). In the feedback model whenever the black hole accretes a sufficient amount of gas to stimulate nuclear activity, the accompanying radiation stimulated by the accretion heats up the hot gas and prevents further cooling. This is supposed to be a cyclical process such that the AGN phase is sufficiently rare to be consistent with the lack of nuclear activity in most cooling flows.

The spectacular radio map of M87 published by Owen et al (2000) shows that radio emission pervades the hot gas of M87 out to radii of $\sim 5'$. The distortions in the *ROSAT* X-ray contours present in annuli #2-3 (Figure 1) testify to the interaction of the radio emission associated with the jet and the hot gas (Harris et al, 2000). The interpretation of the radio emission of M87 in terms of the AGN feedback model has been discussed by Binney (1999).

Our multiphase models of the *ROSAT* PSPC data of M87 appear to support the picture of a standard inhomogeneous cooling flow that has been partially disturbed by the AGN. We focus the reader’s attention on the radial profiles of both \dot{M} for the cooling flow model in Figure 10 and the emission-measure fraction of warm gas in two-phase models shown in Figure 12. In particular, for the cooling flow models \dot{M} is consistent with a constant value for $R > 5'$ appropriate for a standard multiphase cooling flow. But for annuli #2-4 (i.e., $R = 1'$ to $R \sim 4'$) \dot{M} is zero. Over this region lies the asymmetrical features in the X-ray isophotes and the most prominent radio emission from the jet which would seem to support the notion that the AGN has disturbed the cooling flow in this region. In the central bin ($R \leq 1'$) we do see significant cooling (especially for the two-phase models) which is not surprising since the relaxation and cooling times are shortest there, and thus it would be the first to readjust after the disturbance from the AGN.

It should be remembered that the scenario we have described has been based on the *emission* component of the warm gas. The absorption given by the optical depth of the single edge is essentially constant (or declining slowly) with increasing radius. Consequently, although the AGN may have inhibited the cooling of the warm gas in the central regions it apparently has not affected much the absorption properties of the gas. Whether or not this is reasonable requires a more complex model of the warm absorber/emitter than we have employed in this paper (see §6.2). If this description is correct for M87 then it very likely applies to other cooling flows. In this case it will be critical to understand how this process evolves and how ubiquitous it is in cooling flow galaxies, groups, and clusters.

7. CONCLUSIONS

From analysis of spatially resolved, deprojected *ROSAT* PSPC spectra we find the strongest evidence to date for intrinsic oxygen absorption and multiphase gas in the hot ISM/IGM/ICM of a galaxy, group, or cluster. When attempting to describe the 0.2-2.2 keV *ROSAT* emission of M87 by a single-phase hot plasma modified by standard

Galactic absorption the best-fitting model displays striking residuals in the spectrum (Figure 2): (1) excess emission above the model for 0.2-0.4 keV and (2) excess absorption below the model for 0.5-0.8 keV. These features are apparent out to the largest radii investigated (~ 100 kpc) and cannot be attributed to errors in the calibration or the background subtraction (see §4.1).

The principal result is that the 0.5-0.8 keV absorption is consistent with that of a collisionally ionized plasma with a temperature of 10^{5-6} K, where the lack of evidence of absorption below 0.5 keV strongly excludes the possibility of absorption from cold material as has been assumed in essentially all previous studies of absorbing material in cooling flows. In fact, the excess *emission* observed between 0.2-0.4 keV, which is also manifested as sub-Galactic column densities in models with standard (cold) absorbers (§4), has a temperature that is consistent with the emission from gas responsible for the 0.5-0.8 keV absorption and could not be explained if dust were responsible for both the absorption and soft emission. (See section 5.1 of PAPER3 for discussion of other problems with dust.)

Only multiphase models can provide good fits over the entire PSPC bandpass while also yielding temperatures and Fe abundances that are consistent with results from *ASCA* and *SAX* at large radii (§5). Both cooling flow and two-phase models indicate that the fraction of warm gas with respect to the total emission measure differs qualitatively for radii interior and exterior to $\sim 5'$ (~ 26 kpc). For $r > 5'$ the data are consistent with a constant (or slowly varying) fraction of warm gas as a function of radius. But for $r < 5'$ the warm gas fraction varies from $\sim 20\%$ within the central bin ($1'$) to essentially zero within the next few bins (out to $5'$). This behavior is to be contrasted with the absorption optical depth profiles which are approximately constant with radius.

The oxygen absorption and soft emission from warm (10^{5-6} K) gas in M87 we have detected using the *ROSAT* PSPC (0.2-2.2 keV) is also able to satisfy the detections of excess emission with data at lower energies (0.07-0.25 keV) from *EUVE* (§6.3) and the detection of excess absorption at higher energies (0.5-10 keV) from *Einstein* and *ASCA* (§6.2). Previous studies using only *EUVE* data (e.g., Berghöfer et al. 2000) could not decide between a non-thermal and thermal origin for the excess soft emission. Similarly, the previous detections of absorption with *Einstein* (White et al, 1991) and *ASCA* (Allen et al, 2000) could not constrain the temperature of the absorber and always assumed a cold absorber with solar abundances. Even previous studies with *ROSAT* that neglected data below ~ 0.5 keV also could not constrain the temperature of the absorber (Allen & Fabian 1997; Sanders et al. 2000) because of the strong dependence of the inferred absorption on the lower energy limit of the bandpass (see our Figure 2).

Hence, the *ROSAT* detection of intrinsic absorption that is localized in energy (0.5-0.8 keV) is the key piece of evidence for establishing the presence of warm (10^{5-6} K) gas distributed throughout (at least) the central 100 kpc. This evidence for a multiphase ISM in M87 essentially confirms the original detection within the central $\sim 2'$ using the *Einstein* FPCS (Canizares et al, 1982). However, instead

of intrinsic oxygen absorption Canizares et al (1982) inferred a super-solar O/Fe ratio which does not agree with subsequent analyses of M87 using other instruments. The anomalous O/Fe ratio is probably attributed to either calibration error in the FPCS (see Tsai 1994) or to an underestimate of the continuum due to the absorption edges (see end of §6.1).

Although many previous studies have shown that the *ROSAT* data (0.1-2.4 keV) of galaxy clusters rule out large quantities of cold absorbing gas in these systems (e.g., Arabadjis & Bregman 2000), our spatial-spectral deprojection analyses of M87 in this paper and of A1795 in PAPER1 strongly suggest that large quantities of warm ($T_w \sim 10^6$ K) gas are distributed (at least) throughout the central ~ 100 kpc of cluster cooling flows.

The total mass of the warm gas implied by the oxygen absorption is consistent with the amount of matter deposited by an inhomogeneous cooling flow (§6.2). On the other hand, the mass deposition profile (Figure 11) and the profile of warm emission fraction of the two-phase models (Figure 12) indicate that the emission of the warm component is suppressed over $r \sim 1' - 5'$ where the radio emission from the AGN jet clearly distorts the X-ray isophotes (Owen et al, 2000). This coincidence suggests that the AGN has influenced the hot ISM in these central regions and may have suppressed the cooling emission of the warm component (§6.4; see Binney 1999). Within the central arcminute the gas has apparently readjusted and is cooling while at large radii, $r > 5'$, the cooling flow was not disturbed significantly by the AGN. A hybrid model of a standard cooling flow with AGN feedback seems promising for M87.

It is puzzling, however, why the oxygen absorption optical depth does not dip between $R \sim 1' - 5'$ as would be expected if the absorption and excess soft emission arise from the same material. Perhaps this is a result of the simplifications we have employed in this investigation (e.g., see §6.2), and with rigorous consideration of the radiative transfer and the absorption from several ionization states of oxygen (and carbon and nitrogen) a self-consistent description of the multiphase medium will be obtained.

The highly significant detection of intrinsic oxygen absorption in the *ROSAT* PSPC data of M87 confirms the picture of a multiphase warm+hot medium in cooling flows deduced from the lower S/N PSPC data of galaxies and groups in PAPER1 and PAPER3. With new *Chandra* and *XMM* data the spatial distribution of the different phases can be mapped with novel accuracy, and thus the structure and evolution of cooling flows, and the role of AGN feedback, will be elucidated.

I thank D. Liedahl for discussions relating to the accuracy of plasma emission codes and the anonymous referee for helpful comments. This research has made use of data obtained through the High Energy Astrophysics Science Archive Research Center Online Service, provided by the NASA/Goddard Space Flight Center. Support for this work was provided by NASA through Chandra Fellowship grant PF8-10001 awarded by the Chandra Science Center, which is operated by the Smithsonian Astrophysical Observatory for NASA under contract NAS8-39073.

REFERENCES

Allen, S. W., & Fabian, A. C. 1997, MNRAS, 286, 583

Allen, S. W., Di Matteo, T., & Fabian, A. C. 2000, MNRAS, 311, 493

Anders E., & Grevesse N., 1989, *Geochimica et Cosmochimica Acta*, 53, 197

Arabadjis, J. S., & Bregman, J. N., 1999, ApJ, 514, 607

Arabadjis, J. S., & Bregman, J. N., 2000, ApJ, 536, 144

Balucińska-Church, M., & McCammon, D., 1992, ApJ, 400, 699

Beiersdorfer, P., Lepson, J. K., Brown, G. V., Utter, S. B., Kahn, S. M., Liedahl, D. A., Mauche, C. W. 1999, ApJ, 519, L185

Berghöfer, T. W., Bowyer, S., & Korpela, E. 2000, ApJ, 535, 615

Binney, J. J., 1996, in *Gravitational Dynamics* Proc. 36th Herstmonceux conf., ed O. Lahav (Cambridge: Cambridge University Press), 89

Binney, J. J. 1999, in *The Radio Galaxy M87*, ed. H.-J. Röser & K. Meisenheimer, (Springer-Verlag), 136

Binney, J., & Tabor, G. 1995, MNRAS, 276, 663

Böhringer, H. 1997, in *Galactic and Cluster Cooling Flows* ASP Conf. Ser. vol. 115, ed. N. Soker (San Francisco: ASP), 11

Bonamente, M., Lieu, R., & Mittaz, J.P.D. 2000, ApJ, in press (astro-ph/0001128)

Buote, D. A., 1999, MNRAS, 309, 695

Buote, D. A., 2000a, MNRAS, 311, 176

Buote, D. A., 2000b, ApJ, 532, L113 (PAPER1)

Buote, D. A., 2000c, ApJ, 539, 172 (PAPER2)

Buote, D. A., 2000d, ApJ, in press (astro-ph/0001330) (PAPER3)

Buote, D. A., & Fabian, A. C. 1998, MNRAS, 296, 977

Buote, D. A., Canizares, C. R., & Fabian, A. C. 1999, MNRAS, 310, 483

Canizares, C. R., Clark, G. W., Jernigan, J. G., Markert, T. H. 1982, ApJ, 262, 33

Chen, L.-W., Fabian, A. C., & Gendreau, K. C., 1997, MNRAS, 285, 449

Ciotti, L., & Ostriker, J. P. 2000, ApJ, submitted (astro-ph/9912064)

D'Acri, F., De Grandi, S., & Molendi, S., 1998, in *The Active X-ray Sky: Results from BeppoSAX and Rossi-XTE*, ed L. Scarsi et al., (Holland: Elsevier Science) (astro-ph/9802070)

Dixon, W., Hurwitz, M., & Ferguson, H. C., 1996, ApJ, 469, L77

Fabian A. C., 1994, ARA&A, 32, 277

Fabian A. C., 1996, *Science*, 271, 1244

Fabian, A. C., Nulsen, P. E. J., Canizares, C. R. 1984, *Nature*, 310, 733

Fabian, A. C., Hu, E. M., Cowie, L. L., Grindlay, J., 1981, ApJ, 248, 47

Feldman U., 1992, *Physica Scripta*, 46, 202

Harris, D. E., Owen, F., Biretta, J. A., & Junor, W. 2000, in *Proceedings of the Ringberg workshop: Diffuse Thermal and Relativistic Plasma in Galaxy Clusters*, eds. H. Böhringer, L. Feretti, and P. Schuecker, in press (astro-ph/0002464)

Hasinger, G., Boese, G., Predehl, P., Turner, T. J., Yusaf, R., George, I. M., & Rohrbach, G., 1995 *MPE/OGIP Calibration Memo CAL/ROS/93-015 ver. 1995 May 8*

Ishimaru, Y., & Arimoto, N., 1997, PASJ, 49, 1

Johnstone, R. M., Fabian, A. C., Edge, A. C., & Thomas, P. A. 1992, MNRAS, 255, 431

Kaastra, J. S., & Mewe, R., 1993, A&AS, 97, 443

Krolik, J. H., & Kallman, T. R., 1984, ApJ, 286, 366

Liedahl, D. A., 1999, in *Atomic Data Needs for X-ray Astronomy*, eds. M.A. Bautista, T.R. Kallman, A.K. Pradhan, <http://heasarc.gsfc.nasa.gov/docs/heasarc/atomic/>

Liedahl, D. A., Osterheld, A. L., & Goldstein, W. H., 1995, ApJ, 438, L115

Lieu, R., Mittaz, J. P. D., Bowyer, S., Lockman, F. J., Hwang, C.-Y., & Schmitt, J. H. M., 1996, ApJ, 458, L5

Mewe R., Gronenschild E. H. B. M., & van den Oord G. H. J., 1985, A&AS, 62, 197

Morrison, R., & McCammon, D., 1983, ApJ, 270, 119

Nulsen, P. E. J., & Böhringer, H., 1995, MNRAS, 274, 1093

Owen, F. N., Eilek, J. A., & Kassim, N. E. 2000, ApJ, in press (astro-ph/0006150)

Peres, C. B., Fabian, A. C., Edge, A. C., Allen, S. W., Johnstone, R. M., White, D. A. 1998, MNRAS, 298, 416

Pistinner, S., Sarazin, C. L. 1994, ApJ, 433, 577

Sanders, J. S., Fabian, A. C., & Allen, S. W. 2000, MNRAS, in press (astro-ph/0006394)

Snowden, S. L., McCammon, D., Burrows, D. N., & Mendenhall, J. A., 1994, ApJ, 424, 714

Snowden, S. L., Turner, T. J., George, I. M., Yusaf, R., Predehl, P., & Prieto A. 1995, *OGIP Calibration Memo CAL/ROS/95-003*

Stewart, G., Canizares, C. R., Fabian, A. C., Nulsen, P. E. J. 1984, ApJ, 278, 536

Sutherland, R. S., & Dopita, R. S., 1993, ApJS, 88, 253

Tsai, J. C. 1995, ApJ, 429, 119

Voit, G. M., & Donahue, M. 1995, ApJ, 452, 164

White, D. A., 2000, MNRAS, 312, 663

White, D. A., Fabian A. C., Johnstone R. M., Mushotzky, R. F., & Arnaud, K. A., 1991, MNRAS, 252, 72

Yan, M., Sadeghpour, H. R., & Dalgarno, A., 1998, ApJ, 496, 1044